Minimax Theory and its Applications

Volume 12 (2027), No. 1, 34 to 58

An EEG Signal–Based Framework for Early Recognition and Analysis of Stress Using MiniMax-Normalized Discrete Dual-Stream Hopfield Temporal Neural Network with Cosmic Evolution Optimization

Prof. Dong-Jo Kim

Department Image design, School of Animation and Culture Contents, Sunchon National University, Sunchon, Korea, Email: djkim@scnu.ac.kr, 0000-0001-6495-6704

Abstract

Stress has become a widespread health concern affecting cognitive performance, mental well-being, and productivity.Conventional stress assessment methods often depend on subjective self-reports or limited physiological indicators, which may not provide timely or accurate results, whereas EEG signals offer objective insights into brain activity but are complex, noisy, and challenging to analyze effectively. To overcome these challenges, a robust framework called the Discrete Dual-Stream Hopfield Temporal Neural Network with Cosmic Evolution Optimization (DD-SHTNNt+CEO) is suggested for effective early Stress Detection (SD) and analysis. EEG signals are obtained from the SAM 40 and DEAO datasets and initially subjected to preprocessing using the Structure-Preserving Diffusion Model for 3-D Mesh Denoising (S-PDM-3DMD) method to suppress noise and enhance signal quality. Subsequently, informative and discriminative characteristics are derived in accordance with the Quaternion and Clifford Fourier Transforms (Q-CFT) method to efficiently identify the inherent pattern of stress conditions. These extracted characteristics are then fed as inputs to the DD-SHTNNt model, which integrates Discrete Hopfield Neural Network (DHNN) with Dual-Stream Temporal Transformer (D-STT)to achieve accurate classification of stress states. Furthermore, the Cosmic Evolution Optimization (CEO) algorithm is employed to optimally tune the network parameters, thereby enhancing classification performance, accelerating convergence, and improving the overall stability and generalization capability of the suggested framework.The experimental findings demonstrate that the suggested DD-SHTNNt+CEO framework achieves better, significantly more stable performance in SD. The model attains an accuracy of 99.3%, along with 99.1% recall, 99.1% sensitivity, and a 99.1% F1-score, while maintaining a minimal error rate of 0.3% across both datasets. These results indicate that the suggested framework accurately captures stress-specific EEG characteristics, thereby ensuring stable classification, improved generalization, and greater robustness for early SD applications.

Keywords: Cosmic Evolution Optimization, Discrete Hopfield Neural Network, Discrete Hopfield Neural Network, Quaternion and Clifford Fourier Transforms, Stress Detection, Structure-Preserving Diffusion Model for 3-D Mesh Denoising.

1. Introduction

The increasing rate and complexity of contemporary living have heightened both the psychological and environmental demands that necessitate the timely diagnosis of stress as a kind of research subject of increasing significance [1]. Chronic stress is closely linked with various health-related issues, such as heart disease, depressed immunity, anxiety, depression, and mental dysfunction [2]. Beyond its direct influence on productivity, decision-making, and quality of life, the impact of stress on medical outcomes is far-reaching. Timely identification of stress should thus be critical to prevent long-term health consequences and to enable early interventions [3]. However, stress is not clearly defined because it is a complex response involving neural, physiological, and psychological processes. One of the physiological monitoring techniques that has garnered interest is electroencephalography (EEG), which can record electrical activity in the brain [4]. Unlike peripheral measurements, which reflect the organism's secondary responses, EEG provides real-time information on neural activity related to emotional and mental processes. Stress causes apparent alterations in the brainwave activity, particularly in the frequency bands. These changes reflect variations in attention, arousal, and emotional regulation, providing insight into how the brain reacts to stressful stimuli [5]. EEG has a high temporal resolution, allowing continuous recording of rapid neural changes, making it especially effective for identifying transient stress responses in real time. EEG signals, however, are complex and pose special problems for analysis [6]. The nature of brain signals is nonlinear, nonstationary, and extremely sensitive to external artifacts. Moreover, the principles of neural patterns are stress-related, and they differ among individuals due to differences in personality, coping mechanisms, and initial mental states. Similar features require complex computational methods that can construct delicate and dynamic patterns within high-dimensional neural data [7-

8]. In the given instance, deep learning has emerged as a revolutionary paradigm that enables leveraging raw EEG data to learn meaningful representations automatically, without manual feature engineering. Notably, deep learning models are useful for capturing the spatial and temporal characteristics of EEG recordings [9-10]. Scalp electrodes are spatially distributed to reveal the functional relationships between brain regions over time series, thereby showing how cognitive and emotional processes vary over time. Deep neural architectures can learn hierarchical representations and extract patterns of discrimination that match the different degrees of stress intensity [11-12]. This objective methodology strengthens the ability to capture hidden neural patterns that would otherwise be invisible with other methods of analysis. In addition, deep learning models can adapt to large-scale datasets and improve as more data is provided [13]. Deep learning systems based on EEG embedded in stress analysis have enormous potential for individual healthcare and adaptive technologies. Continuous neural monitoring can facilitate proactive stress management in the workplace, academic institutions, as well as clinical settings [14]. It may also help create smarter systems that can dynamically respond to a person's state of mind, thereby fostering feelings about one's emotional health and cognitive performance. With the increasing size and availability of wearable EEG devices, the possibility of real-life stress monitoring is growing [15].
Despite such innovative perspectives, EEG-based stress analysis continues to struggle with issues of signal variability, data quality, computational efficiency, generalization across individuals, limited data diversity, standardization, and model interpretability. This paper discusses and provides solutions to severe research gaps and limitations present in the area.

Novelty as well as contribution
The Novelty as well as the Contribution of the paper is as follows:
❖ **Framework Development**: To create a robust DD-SHTNNt+CEO framework for effective early SDas well as analysis using EEG signals.
❖ **Signal Preprocessing:**To preprocess the EEG Signals of the SAM 40 along with the DEAO databases with the help of the S-PDM-3DMD algorithm to remove noise and improve the quality of signals.
❖ **Feature Extraction**: To extract informative and discriminative features with the Q-CFT method for capturing stress-related patterns.
❖ **Stress Classification Model**: To design the DD-SHTNNt model, DHNN is combined with D-STT to classify stress states correctly.
❖ **Parameter Optimization**: To apply the CEO algorithm to optimally tune network parameters and improve classification efficiency.
The entire manuscript is organized into five sections: a review of the literature in section two; suggested methods in section three; results as well as discussion in section four; and a conclusion and future projects in section five.

2. Related works

The following list includes articles on EEG Signals based on early SD and Analysis utilizing deep learning:
In 2025, Afify, et al [16] has presented a VGGish-CNN model on EEG data from the SAM 40 database, which comprises data from 40 patients, and a signal is captured during four mental tasks to identify short-term stress when the data is input to VGGish as a method of feature extraction. The main aim was to assess the short-term stress levels during such exercises. According to k-fold cross-validation, VGGish-CNN had a higher categorization accuracy (99.25) than its predecessor (99.11). In addition to its role in brain-computer interface (BCI) application development, this study opens the door to further studies using EEG data to help identify mental illnesses and support neurorehabilitation.
In 2025, Shikha, et al [17] has introduced two new features of the KRAFS-ANet framework to enhance stress classification on wearable device EEG data: ensemble stacking with bagging Support Vector Machine, bagging Random Forest, along with bagging K-Nearest Neighbor, with an Artificial Neural Network meta-classifier, and channel selection using Normal Mutual Information and Recursive Feature Elimination. Additional testing (MAT database) produced 98.63% and 98.82% accuracy with 98.63% as well as 98.82% F1-scores, respectively, despite the SAM40 and DASPS datasets reporting 97.25% and 94.92%, respectively.The framework enhances the application of EEG-stress detection in wearables and smartphones to improve mental health by enabling real-time stress monitoring, in addition to interventions.
In 2026, Naren, et al [18] has presented a 1D-CNN framework for EEG signals from subjects under stress, which serves as a system for stress classification. The system can generate phase-controlled bi-channel adaptive features using a least-mean-square adaptive filtering method that changes feature amplitudes based on phase changes. A 1D-CNN model is then used to classify the features into stress types (medium, low, and high). The special dual-activation and dual-pooling structure of the 1D-CNN employs positive and negative activation functions to promote feature preservation. The evaluation is performed using the SAM-40 dataset, which yields positive values for classification precision and recall.
In 2025, Bamanikar, et al [19] has presented U-AGGDCNet+SAO, a successful DL architecture for detecting early stress to address EEG analysis issues. It is a multiple-discrete orthonormal S-transform for feature extraction, a snow ablation tuned uncertainty-aware gated graph decision capsule network for characterization,

and an iterative, robust, peak-aware guided filter for EEG denoising. The hybrid approach improves statistical stability and signal clarity with an error of 0.1, 99.9% accuracy, as well as 98.8% F1-score on the SAM40, along with DEAP databases. Due to its reliability and generalizability, the framework could serve as a valuable tool for early stress monitoring using EEG measurements.

In 2025, Dhake, et al [20] has introduced an algorithm (ISMO-WPT-DCNN) that uses the 2-D wavelet packet transform (WPT) alongside deep convolutional neural networks (DCNNs) to identify mental stress; it improves temporal representation and feature distinguishability. The study proposes two learning strategies for the augmented Spider Monkey Optimization (ISMO) to increase solution diversity and convergence. On the DEAP dataset, the ISMO-WPT-DCNN model achieves 97.54% accuracy, 0.99 recall, 0.95 precision, and 0.97 F1-score, outperforming previous methods.

In 2023, Mane, et al [21] has presented a new StressNet architecture, which is a long short-term memory (LSTM) network along witha two-dimensional CNN to detect stress states in EEG signals. The LSTM leverages its ability to forecast temporal dynamics to examine the alpha, beta, and theta components of EEG data, which are then converted into azimuthally projected images to extract features. StressNet consists of fully connected layers that categorize features as either stress or normal. StressNet is more effective than human detection and achieves a stress detection rate of 97.8 percent on the DEEP and SEED datasets.

In 2022, Hamatta, et al [22] has presented an ECNN-LSTM system that explores wearable computing and deep learning to detect stress across a wide range of contexts, including travel and education, using devices such as EEG, PPG, and GSR. The ECNN-LSTM model is used to classify the DEAP dataset, and the genetic algorithm features are extracted. Signal artifacts are removed by using preprocessing techniques. At a particular level of stress, an alert state is generated.Finally, the findings were compared to conventional techniques using accuracy, F1-score, precision, and recall.

In 2022, Joshi, et al [23] has presented a D-RNN-BiLSTM algorithm for EEG-based emotion classification. Some significant differences between the datasets include EEG devices, stimuli, and cultural influences. Various models, trained with PSD, Hjorth parameters, DE, and LF-DE, were used. There was also a significant improvement in recognition accuracy: 8.2 when training on DEAP and testing on SEED, and 1.5 when training on SEED and testing on DEAP. Emotion detection can be significantly improved by optimizing deep neural network settings, and the results showed that LF-DE using BiLSTM is considerably better than other features and classifiers.The general summary of the existing techniques is described in Table 1.

Table 1: The general summary of the current methods

References	Methods	Advantages	Disadvantages
Afify et al., 2025 [16]	VGGish-CNN	Effective feature extraction using VGGish. Strong k-fold cross-validation performance.	Assessed using the SAM40 dataset only. It can be that deep architecture is computationally intensive.
Shikha et al., 2025 [17]	KRAFS-ANet	Ensemble stacking improves classification robustness. Suitable for wearable and smartphone-based monitoring.	Higher computational complexity. May require careful hyperparameter tuning.
Naren et al., 2026 [18]	1D-CNN	Activation and pooling reduce the feature loss associated with dual activation. Phases have different levels of stress intensity.	Adaptive filtering increases preprocessing time.Partially unvalidated moderate generalizability.
Bamanikar et al., 2025 [19]	U-AGGDCNet +SAO	High-end de-ionization and optimization. High statistical stability.	Heavy computational requirements. Implementation difficulty for real-time wearable systems.
Dhake et al., 2025 [20]	ISMO-WPT-DCNN	Strong temporal representation via 2D-WPT. Improved optimization via ISMO.	The optimization algorithm reduces the time required for training. Very little real-world validation of wearables.
Mane et al., 2023 [21]	StressNet	Combines spatial & temporal modelling. Uses azimuthal projection for image-based features.	EEG converts images to a format that can be converted (image processing). Higher memory consumption.

Hamatta et al., 2022 [22]	ECNN-LSTM	Segmentation of genetic algorithm features. Applicable in the traveling and school setting.	A multi-sensor system is more expensive in terms of hardware. GA increases computational overhead.
Joshi et al., 2022 [23]	D-RNN-BiLSTM	Improved generalization performance. Significant gain with LF-DE and BiLSTM.	Focused more on emotion classification than direct stress. Performance is dependent on feature selection.

Problem statement

Timely stress identification remains a priority for avoiding long-term psychological and physiological health problems. According to global health reports, a significant proportion of the population experiences stress-related conditions that negatively affect mental well-being, productivity, and overall quality of life. Nevertheless, maximal attention should be paid to early stress detection, as brain activity, measured through EEG signals, is highly dynamic. The EEG statistics are highly non-stationary, noisy, and susceptible to external and internal interference, making their correct interpretation difficult. Traditional methods of detecting stress often fail to detect small changes in nerve activity associated with the initial phases of stress. Besides, stress analysis becomes even more challenging because individual differences and the high dimensionality of EEG signals can lead to unreliable results. Hence, there is an urgent need for an efficient framework capable of effectively analyzing EEG signals and detecting early stress patterns, enabling timely and more effective responses to neural indicators of stress.

3. Proposed methodology

This section outlines the architecture of the Discrete Dual-Stream Hopfield Temporal Neural Network with Cosmic Evolution Optimization (DD-SHTNNt+CEO) of the EEG signal analysis and the SD. To begin with, raw EEG data are preprocessed using the S-PDM-3DMD method to remove noise and improve signal quality. After that, the Q-CFT technique is used to extract informative and discriminative features. The obtained features are then input into the DD-SHTNNt model to appropriately classify stress conditions. Lastly, the CEO algorithm is used to optimize network parameters, thereby enhancing classification, convergence, and overall model stability. Figure 1 demonstrates the general scheme of the suggestedDD-SHTNNt+CEO model.

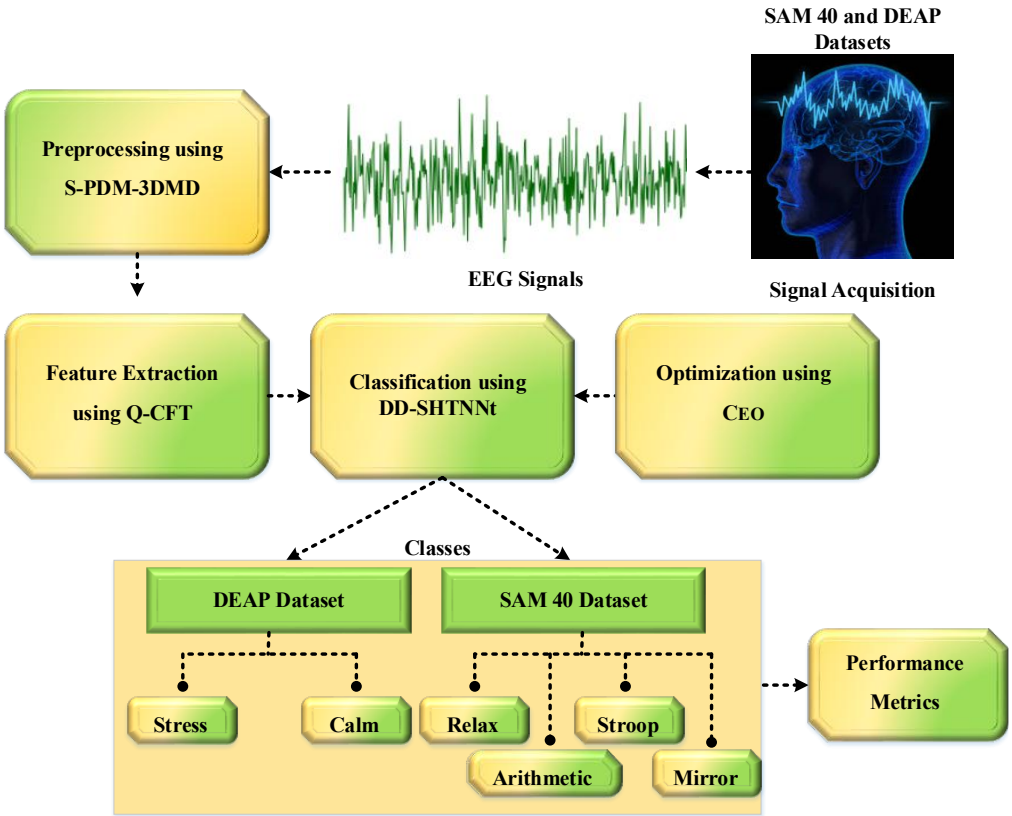


Figure 1: The overall workflow of the suggested DD-SHTNNt+CEO framework

3.1. Signal Acquisition

The input EEG signals are sourced from the SAM40 as well as DEAP databases, which are commonly used for stress and emotion analysis. These datasets provide reliable EEG recordings reflecting variations in cognitive and emotional states. The acquired EEG signals are then forwarded to the preprocessing stage, as described below, to remove noise and improve signal quality.

3.2. Preprocessing using Structure-Preserving Diffusion Model for 3-D Mesh Denoising (S-PDM-3DMD)

EEG signals of SAM40 and DEAP are preprocessed with an S-PDM-3DMD [24] to detect early stress. Within this scheme, EEG electrodes are overlaid on a 3-D scalp mesh, with each vertex representing an electrode characteristic (e.g., band power or differential entropy), and mesh connectivity captures the spatial association between channels.

To remove noise without collapsing the spatial structure of EEG electrodes, a modified forward diffusion process is applied. Unlike conventional diffusion that shrinks the structure, the proposed method adds Gaussian noise while preserving electrode geometry as given by equation (1):

$$b\left(a_l \middle| a_{l-1}\right) = \xi\left(a_l; a_{l-1}, \Im_l L\right) \tag{1}$$

where, a_{l-1} is anEEG mesh vertex at timestep $l-1$, a_l is a noisy EEG mesh vertex at timestep l, $\xi(\cdot)$ is a Gaussian distribution, $\Im_l$ is a variance schedule controlling noise intensity, L is an identity matrix (independent noise per vertex), l is a diffusion timestep.This formulation ensures that noise is injected around the scalp manifold rather than distorting the spatial arrangement of electrodes, which is crucial for stress-related spatial pattern analysis. At any diffusion timestep, the noisy EEG mesh representation can be expressed as equation (2):

$$a_l = a_0 + \sqrt{\overline{\Im}_l}\wp \quad where, \wp \approx \xi(0,1) \tag{2}$$

where, a_0 is an original clean EEG mesh feature, $\sqrt{\overline{\Im}_l}\wp$ is a cumulative noise variance, $\wp$ is a standard Gaussian noise, $\overline{\Im}_l$ is a noise scaling factor. This step simulates progressive corruption of EEG signals while keeping the structural topology intact. The model then learns to recover the clean EEG representation through reverse diffusion. The denoised vertex estimation at timestep is given by equation (3):

$$a_{l-1} = a_l - \frac{\Im_l}{\sqrt{\overline{\Im}_l}}\wp_\infty(a_l, l) \tag{3}$$

where, $\wp_\infty$ is the learned noise predictor, a_{l-1} is a recovered (denoised) EEG vertices, ∞ is a learnable network parameter. This reverse process gradually removes noise from EEG features while maintaining spatial smoothness and electrode connectivity.

S-PDM-3DMD preprocessing is an EEG signal preprocessing method that improves signal quality by applying a structure-preserving diffusion on a 3-D scalp mesh. It eliminates noise, preserves electrode topology, enhances spatial uniformity, and improves the presentation of stress-related features, thereby enabling the identification and analysis of the initial signs of stress. Such processed signals are then sent to the feature extraction stage.

3.3. Feature Extraction using Quaternion and Clifford Fourier Transforms (Q-CFT)

Feature extraction is the process of transforming raw data into useful, compact representations that enhance the ability to recognize and classify patterns. In EEG-based early stress analysis, frequency-domain features are obtained using Q-CFT [25], thereby preserving spatial and phase correlations across channels. These hypercomplex transforms do not lose the geometric structure or inter-channel coupling, as in classical Fourier analysis, and are essential for identifying the minute changes in brain activity induced by stress.

For a quaternion-valued signal, the two-sided Quaternion Fourier Transform is defined as equation (4):

$$E(\nu_1, \nu_2) = \int_{-\varpi}^{\varpi}\int_{-\varpi}^{\varpi} s^{a\nu_1 l_1} j(l_1, l_2) s^{b\nu_2 l_2} g l_1 g l_2 \tag{4}$$

where, $j(l_1, l_2)$ is a quaternion-valued EEG signal, l_1, l_2 is a time (or spatial) variable, a, b is a quaternion imaginary unit, ν_1, ν_2 is an angular frequency variable, $s^{a\nu_1 l_1}$ and $s^{b\nu_2 l_2}$ are quaternion exponential kernels, $E(\nu_1, \nu_2)$ is a quaternion frequency spectrum, $g l_1 g l_2$ is a differential area element for double integration.From the quaternion spectrum, stress-sensitive features such as spectral magnitude, band power, and inter-channel phase coupling can be extracted.For a multivector signal, the Clifford Fourier Transform is expressed as equation (5):

$$\xi_m\{p\}\{\nu\} = \int_{\mathrm{B}^m} p(w) s^{-a_m w\cdot\nu} g^m w \tag{5}$$

where, $p(w)$ is a multivector EEG signal, w is an m-dimensional signal variable, v is an m-dimensional frequency vector, $w \cdot v$ is an inner (dot) product, $s^{-a_m w \cdot v}$ is aclifford exponential kernel, $g^m w$ is a m-dimensional integration measure, $\xi_m \{p\}\{v\}$ is a clifford spectrum. From this transform, spatial–frequency energy distributions and multichannel spectral coefficients are extracted for stress characterization.
A one-sided Clifford Fourier Transform is given by equation (6):

$$\xi_m \{q\}\{v\} = \int_{B^m} q(w) s^{-a_m w \cdot v} g^m w \quad (6)$$

where, $q(w)$ is a multivector EEG function, $\xi_m \{q\}\{v\}$ is a one-sided Clifford spectrum. The exponential kernel allows directional frequency analysis while preserving geometric structure.From this representation, scalar spectral energy, directional components, and multivector frequency coefficients are derived as discriminative features for early stress detection.
The Q-CFT produces structured multichannel frequency representations while retaining information on geometries and phases. The features extracted, such as band energy, spectral magnitude, and spatial-frequency coupling, are useful for describing EEG stress patterns and for improving the ability to distinguish between early stress conditions. These extracted features are then provided to the classification stage.

3.4. Classification using Discrete Dual-Stream Hopfield Temporal Neural Network (DD-SHTNNt)

Following the feature extraction process, the DD-SHTNNt framework is used to perform early stress-state classification of the extracted EEG features. The model combines the strengths of a Discrete Hopfield Neural Network (DHNN) with a Dual-Stream Temporal Transformer (D-STT) to extract both associative memory patterns as well as temporal dependencies inherent in EEG signals. The DHNN component assists in stabilizing and refining feature representations, while the D-STT module analyzes temporal variations through parallel processing streams. Combined, these factors enhance the model's ability to identify subtle patterns of stress. The detailed architecture of the DD-SHTNNt model is described below, and the complete layer-wise structural diagram is illustrated in Figure 2.

3.4.1. Discrete Hopfield Neural Network (DHNN)

The DHNN [26] divides EEG stress patterns using symmetrical synaptic weights, neuron update thresholds, and minimizing Lyapunov energy. The Boltzmann probability increases the stability of convergence. The lowest-energy state defines the stress or non-stress states in the SAM40 and DEAP databases.

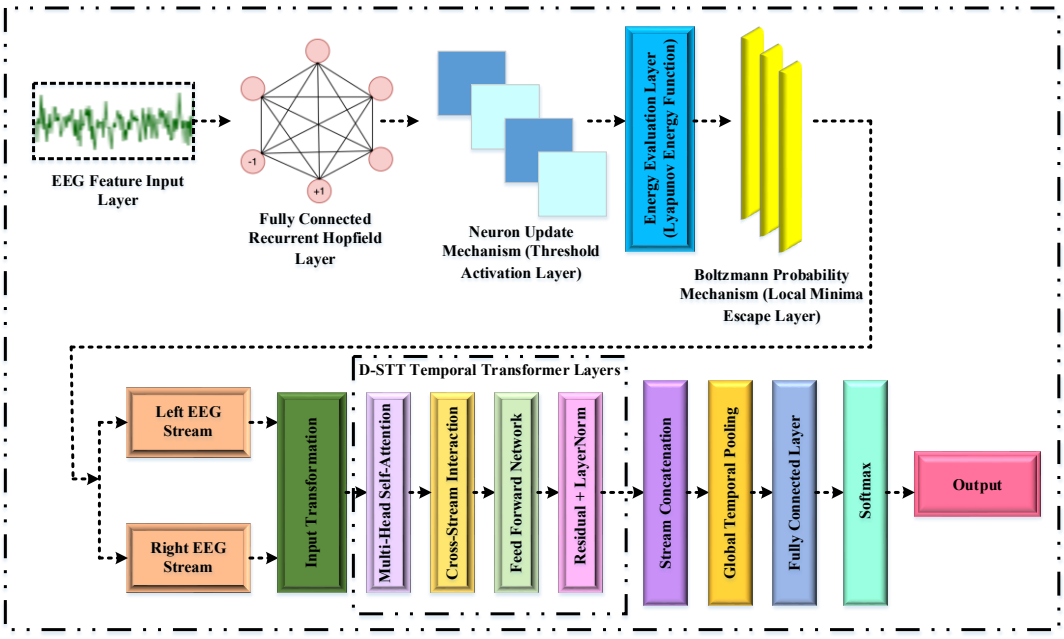


Figure 2: The complete layer-wise structural diagram of the DD-SHTNNt model

During classification, the network uses trained weights that satisfy the structural constraint, as given by equation (7):

$$V_{ab}^{(2)} = V_{ba}^{(2)}, V_{aa}^{(2)} = V_{bb}^{(2)} = 0 \quad (7)$$

where, $V_{ab}^{(2)}$ is a second-order synaptic weight between neuron a and b, $V_{ba}^{(2)}$ is a weight parameter, $V_{aa}^{(2)}, V_{bb}^{(2)}$ is a self-connection weight (set to zero). This means the connections between neurons are symmetric, and no neuron connects to itself. This property guarantees stable convergence of the network during stress classification.

The classification decision is made by updating neuron states based on the weighted input is given by equation (8):

$$C_a^{fi} = \begin{cases} 1, & \sum_{b=1,a\neq b}^{M} V_{ab}^{(2)} + V_a^{(1)} \geq \beta \\ 1, & \sum_{b=1,a\neq b}^{M} V_{ab}^{(2)} + V_a^{(1)} \leq \beta \end{cases} \quad (8)$$

where, C_a^{fi} is the final state of the neuron a, $V_{ab}^{(2)}, V_a^{(1)}$ are second- and first-order weights, β is the bias vector, M is the total number of neurons (features). The network iteratively updates all neurons until no further changes occur.After convergence, the stability of the classified EEG pattern is evaluated using the Lyapunov energy function. The measure of this energy is the stability of the final pattern of stress or non-stress. When energy is low, it indicates a more stable and reliable classification.

In case of the network having locked the local minimum during categorization, the probability of flipping the neuron state is calculated based on equation (9):

$$r_a = \frac{1}{1 + o^{\frac{K}{L}}} \quad (9)$$

where, K is the energy difference, L is the temperature parameter, r_a is the probability of flipping a neuron a, o is an exponential constant. Higher temperature increases the likelihood of overcoming local minima, thereby improving the performance of stress classification.

DHNN-based EEG stress classification recalculates neuron states using trained symmetric weights, and stability is measured by energy minimization. Boltzmann probability enhances convergence in the case of local minima. The consistent minimum-energy state denotes precise stress or non-stress detection of SAM40 as well as DEAP databases.

3.4.2. Dual-Stream Temporal Transformer (D-STT)

D-STT [27] is intended to directly classify stress using two streams of EEGs. The architecture does not emphasize feature extraction; rather, it aims to learn a discriminative temporal representation and predict stress labels. The two streams can be hemispheric EEG channels or time-domain features, and thus the two streams enable the model to capture inter-channel stress correlations.

The dual EEG streams are first mapped into a classification feature space is given by equation (10):

$$E_T^0, E_P^0 = K^{conv}(W_T), K^{conv}(W_P) \quad (10)$$

where, W_T, W_P denote left and right EEG streams, $K^{conv}(\cdot)$ is the input transformation layer E_T^0, E_P^0 are initial classification representations. This step prepares EEG sequences for temporal classification learning. The D-STT layers learn temporal dependencies and exchange information across streams to strengthen stress discrimination, as given by equation (11):

$$E_T^{(a)}, E_P^{(a)} = \begin{cases} K_T^{C_a}(E_T^{(0)}), K_P^{C_a}(E_P^{(0)}) & a = 1, \\ K_T^{C_a}(E_T^{(a-1)} \Theta E_P^{(a-1)}), K_P^{C_a}(E_P^{(a-1)} \Theta E_L^{(a-1)}), & a = 2,3,...,M_a \end{cases} \quad (11)$$

where, $K_T^{C_a}$ represents the $a-th$ temporal transformer layer, M is the total number of layers, Θ denotes concatenation, $E_T^{(a)}, E_P^{(a)}$ is an updated classification feature, a is a transformer layer index. This mechanism captures long-range temporal stress patterns and cross-stream interactions. After stacked transformer layers, the final classification-oriented representations are obtained as given by equation (12):

$$E_T^c, E_P^c = K^C(E_T^0, E_P^0) + E_T^0, E_P^0 \quad (12)$$

where, K^C denotes the complete D-STT classification module, E_T^c, E_P^c is a final stress-aware feature representation. These representations encode discriminative stress-related EEG dynamics across time. The final stress prediction is performed through a classification layer, as given by equation (13):

$$E_T^{cl}, E_P^{cl} = K^L(E_T^c, E_P^c) \quad (13)$$

where, K^L is the classification layer, E_T^{cl}, E_P^{cl} is a final stress-aware representation, E_T^c, E_P^c are predicted stress labels. By minimizing a categorization error between the true as well as predicted stress categories, the model is trained. For SAM 40, stress labels correspond to emotional conditions, while in DEAP, stress states are derived from arousal–valence combinations.

D-STT is an improvement of stress classification that combines dual-stream temporal learning and inter-channel correlation modeling. The transformer-based architectures capture long-range EEG dynamics and reconstruct a sound stress representation that facilitates reliable early SD on the SAM 40 and DEAP datasets.

The extracted EEG features are used to classify early stress states using the DD-SHTNNt model. It combines a DHNN and a D-STT to learn the associative patterns of features and temporal variations in EEG signals, thereby enhancing the accuracy and reliability of early SD. The algorithm for improving prediction is then based on the CEO to optimize the DD-SHTNNt model's parameters. Such optimization improves the model's learning ability and overall classification accuracy. The operational procedures and functioning of the CEO-based optimization strategy are presented in the section below.

3.5. Optimization using Cosmic Evolution Optimization (CEO)

The DD-SHTNNt model is optimized using the CEO [28] algorithm to improve classification accuracy while reducing computational cost, processing time, and model complexity. The CEO modulates the principles of universal evolution to maximize the hyperparameters of DD-SHTNNt. The development of candidate solutions is based on expansion, gravitational alignment, collision perturbation, and resonance refinement. The algorithm strikes a balance between world exploration and world exploitation, where classification performance improves until it converges on an optimal hyperparameter setting. The generalization of the CEO's optimization process, as illustrated in Figure 3, outlines the sequence of actions and the timeframe of the practice, as described in the following subsections.

Step 1: Initialization

The candidate solutions are vectors of DD-SHTNNt hyperparameters. This ensures that all DD-SHTNNt hyperparameters are randomly sampled within the specified range. The random initialization of each candidate is defined as given by equation (14):

$$W = rnd(M, \dim) \times (ur - lrd) + lrb \tag{14}$$

where, $rnd(M, \dim)$ is a uniform random number, ur, lrd is an upper and lower bound, W is a $a-th$ candidate hyperparameter vector, a is a population index, M is the total number of candidates.

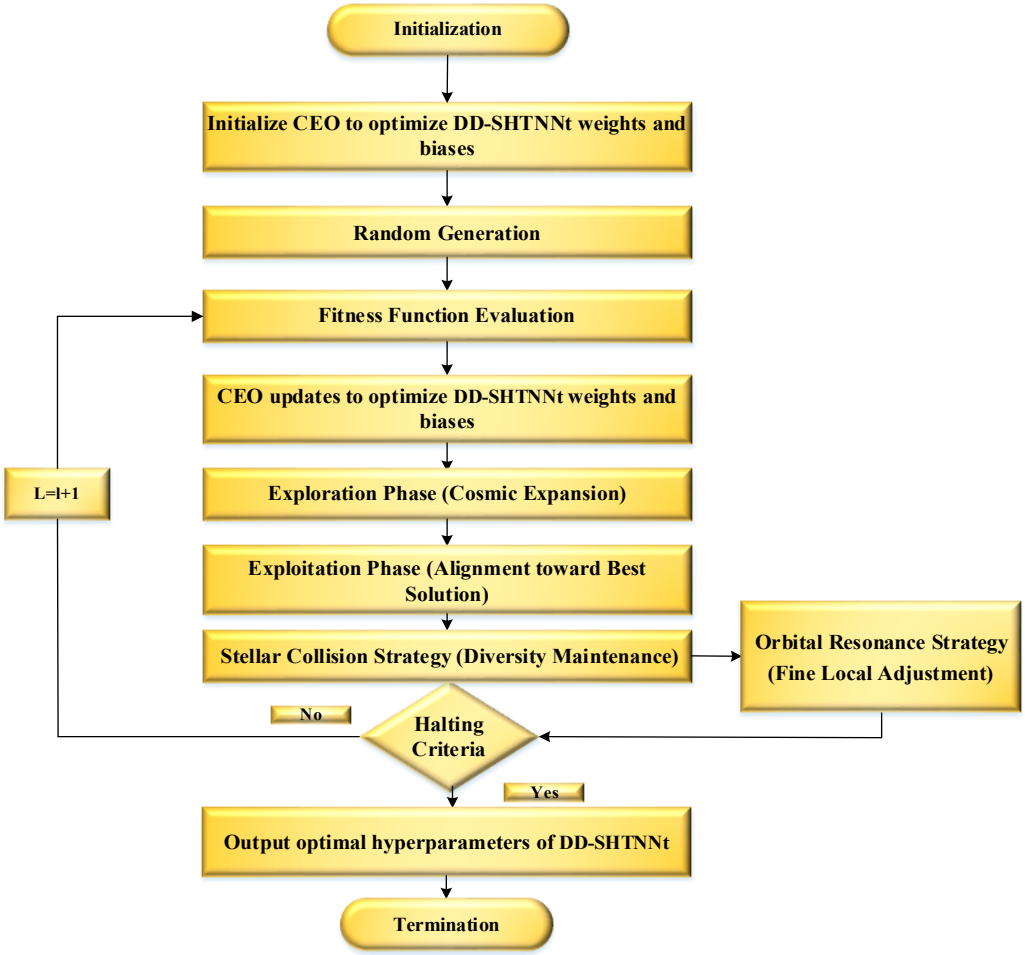


Figure 3: The flowchart of the CEO-based optimization process

Step 2: Random Generation

Random initialisation assigns different hyperparameter combinations, subject to predetermined limits, using a uniform distribution. This is to ensure comprehensive coverage of the search space to avoid early bias toward particular spaces, and to increase the likelihood of finding globally optimal configurations.

Step 3: Assessment of the Fitness Function

Each candidate solution is used to train the DD-SHTNNt model, and its classification performance is evaluated to determine its fitness value. The fitness criterion (f_{it}) is designed to simultaneously minimize the classification error rate while maximizing the overall classification accuracy, as defined in equation (15):

$$f_{it} = \min imize(\beta) \max imize(V_{ba}^{(2)}) \quad (15)$$

where, β effectively reduces computational cost, error, processing time, and overall model complexity while $V_{ba}^{(2)}$ improving classification performance and predictive accuracy.

Step 4: Exploration Phase(Cosmic Expansion)

During exploration, the candidates travel randomly at an adaptive cosmic expansion velocity. Large search steps are performed at the beginning to explore a wide range of hyperparameters. With successive iterations, growth becomes less pronounced, which decreases the search radius and allows targeted refinement.

During early iterations, the CEO performs a global search to explore diverse hyperparameter combinations.The adaptive expansion velocity for the candidate at iteration l is given by equation (16):

$$U_{\exp}(l) = Z_1 \times \left(1 - 0.001 \times \frac{l}{L}\right) \times s^{\frac{4l}{L}} \quad (16)$$

where, l is a current iteration, L is a maximum iteration, Z_1 is an expansion decay constant, $U_{\exp}(l)$ is an expansion velocity of the candidate a. The position update of the candidate becomes, as given by equation (17):

$$W_a(l+1) = W_a(l) + U_{\exp}(l) rndm(\cdot) \times (urb - lrb) \quad (17)$$

where, $rndm(\cdot)$ is a Gaussian random vector, $W_a(l)$ is a current hyperparameter vector, $W_a(l+1)$ is an updated vector, urb, lrb is a search range.

Step 5:Exploitation Phase(Alignment toward Best Solution)

The goal of the exploitation is to ensure that all the candidates are aligned with the best set of hyperparameters. The adaptive alignment coefficient grows slowly, reinforcing attraction to the optimal solution. In the exploitation stage, each candidate moves toward the best hyperparameter configuration $W_{bst}(l)$.The alignment direction for the candidate is given by equation (18):

$$\vec{c}_a(l) = W_{bst}(l) - W_a(l) \quad (18)$$

where, $\vec{c}_a(l)$ is a direction toward the best solution, $W_{bst}(l)$ is thebest candidate at iteration l, $W_a(l)$ is a current hyperparameter vector. The updated position becomes as given by equation (19):

$$W_a(l+1) = W_a(l) + U_{\exp}(l) rndm(\cdot) \times (urb - lrb) + E(l) + B(l) \quad (19)$$

where, $B(l)$ is a direction toward the best solution, $E(l)$ is an adaptive alignment weight.This strengthens fine-tuning of hyperparameters near the optimal region as iterations increase.

Step 6: Stellar Collision Strategy (Diversity Maintenance)

To avoid premature convergence, the candidate may undergo a collision-based perturbation.The collision probability for the candidate is given by equation (20):

$$W_{new} = W_a + \vartheta \cdot \overline{P} \quad (20)$$

where, ϑ is a Gaussian random scalar, $\overline{P}$ is an average search radius, W_a is a current hyperparameter vector of the $a-th$ candidate, W_{new} is an updated hyperparameter vector after collision.

Step 7: Orbital Resonance Strategy (Fine Local Adjustment)

The CEO uses small resonance-based perturbations to escape local minima. If the updated solution improves fitness is given by equation (21):

$$W_a(l+1) = W_{reason}(l+1) \quad (21)$$

where, $W_{reason}(l+1)$ is a resonance-adjusted candidate, enabling fine-grained hyperparameter refinement.

Step 8: Termination

When the maximum number of iterations $(L = l+1)$ is reached, or the fitness improvement falls below a set convergence threshold, the optimization is terminated.

In summary, the suggested DD-SHTNNt+CEO model is a powerful model for early SD of EEG signals. The plan involves preprocessing data with S-PDM-3MD to improve signal quality, extracting features with Q-CFT to identify significant patterns, classifying with DD-SHTNNt to achieve accurate classification, and parameter optimization with CEO to improve model convergence and stability. These components have been successfully incorporated into the model to ensure it is highly accurate, robust, and reliable in operation.A thorough study and a general performance assessment of the suggested framework are covered in the following parts.

4. Results and discussions

This section presents the experimental results along with a detailed discussion of the suggested DD-SHTNNt+CEO framework for Early SD and analysis using EEG signals. The model is implemented and tested in Python, focusing on classification accuracy, computational efficiency, robustness, and reliability. A thorough performance analysis is conducted to ensure its efficiency in early stress detection. Table 2 illustrates the significant simulation environments, network topologies, and implementation specifications applied during the experimental study.

Table 2: Simulation parameters

Category	Component	Setting / Description
Software Environment	Programming Language	Python
	Python Version	3.7.14
	Deep Learning Framework	TensorFlow / Keras
	Supporting Libraries	NumPy, SciPy, Scikit-learn, Pandas, Matplotlib
	Operating System	Windows 10 (64-bit)
Hardware	Processor	Intel Core i7 (3.4 GHz or higher)
	RAM	16 GB

Environment	GPU	NVIDIA GTX 1080 Ti / RTX 2080 (11 GB VRAM)
	CUDA / cuDNN	CUDA 11.x, cuDNN compatible version
Dataset Settings	Datasets Used	SAM 40, DEAP
	Train/Test Split	80% Training / 20% Testing
	Cross-Validation	5-fold (where applicable)
	Data Type	EEG Signals
Training Settings	Batch Size	32
	Epochs	100
	Optimizer	CEO
	Learning Rate	0.001

4.1. Dataset description

The section presents the suggested Early SD analysis framework using EEG signals, which was verified on both the SAM 40 as well as DEAP datasets. The format, data structure, and meaningful features of these datasets are thoroughly explained in the following subsections. Table 3 shows the detailed Description of both datasets.

Table 3: Detailed Description of Dataset 1 as well as Dataset 2

Parameter	**Dataset 1**	**Dataset 2**
Number of Participants	40 healthy subjects	32 subjects (14 selected for balanced calm–stress analysis)
Gender Distribution	26 males, 14 females	16 males, 16 females
Age Range / Mean Age	Mean age: 21.5 years	Age range: 19–37 years
EEG Acquisition System	32-channel EmotivEpoc Flex gel-based headset	32-channel BiosemiActiveTwo system
Electrode Placement	International 10–20 system	International 10–20 system
Sampling Frequency	128 Hz	512 Hz
Experimental Protocol	Relaxed state and three stress tasks: arithmetic solving, Stroop color–word test, symmetric mirror image identification	40 one-minute music video clips to elicit different emotional states
Trial Duration	25 seconds per task (each repeated three times)	63 seconds per trial (including 3-second baseline)
Subjective Ratings	1–10 stress rating scale after each trial	9-point scale for valence, arousal, dominance, and liking
Data Split for Model Development	80% training, 20% testing	80% training, 20% testing

4.1.1. SAM 40 Dataset (Dataset 1) [29]

The dataset 1 is a publicly available EEG dataset developed for SD and cognitive workload analysis. It includes EEG recordings from 40 healthy people (26 males as well as 14 females, mean age 21.5 years) recorded with a 32-channel EmotivEpoc Flex gel-based headgear set up according to the international 10-20 system. The signals were preprocessed to eliminate artifacts and captured at 128 Hz.Each participant performed four conditions: a relaxed state and three stress-inducing tasks, including solving arithmetic problems, performing the Stroop color–word test, as well as identifying symmetric mirror images. Each task lasted 25 seconds and was repeated three times per subject. After each trial, participants rated their perceived stress level on a 1–10 scale, enabling both binary (relaxed vs. stressed) and multi-class (different stress types) classification. The dataset is widely used in deep learning studies for stress recognition and EEG-based biometric identification.

4.1.2. DEAP Dataset (Dataset 2) [30]

The dataset 2 is a publicly available dataset developed for emotion analysis using EEG and peripheral physiological signals. It consists of a recording of 32 subjects (16 men and 16 women, aged 19 to 37) who watched 40 one-minute music videos designed to elicit different emotions. EEG data were recorded at a 512Hz sample rate using 32 electrodes in accordance with the 10-20 system. Emotional state was rated on valence, arousal, dominance, and liking using a 9-point scale every 63 seconds, with a 3-second baseline. In the given analysis, the calm and stress states were defined in terms of valence and arousal thresholds, offered by equations (22 and 23):

$$cm = (arousal < 4) \cap (4 < valence < 6) \quad (22)$$

$$stss = (arousal > 5) \cap (valence < 3) \quad (23)$$

where, $\cap$ is the logical AND operator, cm is the calm, $stss$ is the stress. Based on these criteria, 14 participants (IDs: 2, 4, 10, 11, 12, 13, 15, 16, 20, 21, 22, 25, 31, and 32) with a balanced number of calm and stress trials were included in the study.

4.2. Performance metrics

The effectiveness of the suggested DD-SHTNNt+CEO framework is comprehensively compared with several available benchmark models to confirm its validity. The comparative analysis for Dataset 1 includes VGGish-CNN [16], KRAFS-ANet [17], 1D-CNN [18], U-AGGDCNet+SAO [19], as well as ISMO-WPT-DCNN [20]. Similarly, in the example of Dataset 2, the proposed methodology is compared with U-AGGDCNet+SAO [19], ISMO-WPT-DCNN [20], StressNet [21], ECNN-LSTM [22], as well as D-RNN-BiLSTM [23]. The analysis is conducted using computational and statistical performance measures. These are the computational time, classification accuracy, precision, specificity, recall, sensitivity, error rate, and F1-score. Mathematical forms of these quantitative indicators are presented in Table 4, and their theoretical approaches and specific explanations are provided in the subsequent subsections.

True Positive (∂_{ps}) **:** Correctly identifies the presence of early stress from EEG signals when stress is actually present.

False Positive (τ_{ps}) **:**Incorrectly classifies EEG signals of a relaxed or non-stressed individual as stressed when no stress condition exists.

False Negative (τ_{nt}) **:**Fails to detect early stress from EEG signals when the individual is actually experiencing stress.

True Negative (∂_{nt}) **:**Correctly recognizes EEG signals of a relaxed or non-stressed individual as non-stress in the absence of stress.

Table 4: Performance metrics as well as the equation

Performance metrics	**Equations (24-29)**
Accuracy	$\frac{\partial_{ps}+\partial_{nt}}{\partial_{ps}+\partial_{nt}+\tau_{ps}+\tau_{nt}}$ (24)
Precision	$\frac{\partial_{ps}}{\partial_{ps}+\tau_{ps}}$ (25)
Recall	$\frac{\partial_{ps}}{\partial_{ps}+\tau_{nt}}$ (26)
Specificity	$\frac{\partial_{nt}}{\partial_{nt}+\tau_{ps}}$ (27)
Sensitivity	$\frac{\partial_{ps}}{\partial_{ps}+\tau_{nt}}$ (28)
F1-score	$\frac{2\times(p_{\wp}\times r_{\lambda})}{p_{\wp}+r_{\lambda}}$ (29)

where, $p_{\wp}$ denotes the precision, r_{λ} represents the recall.

4.3. Evaluation of the performance of the suggested techniques

This section presents a comprehensive evaluation of the DD-SHTNNt+CEO framework, demonstrating its effectiveness for early SD and analysis using EEG signals.

4.3.1. Performance analysis of Dataset 1

The following section summarizes the performance evaluation results achieved for Dataset 1, and the figure 4 shows the output result of the suggested method on Dataset 1 for the Arithmetic Task Class.

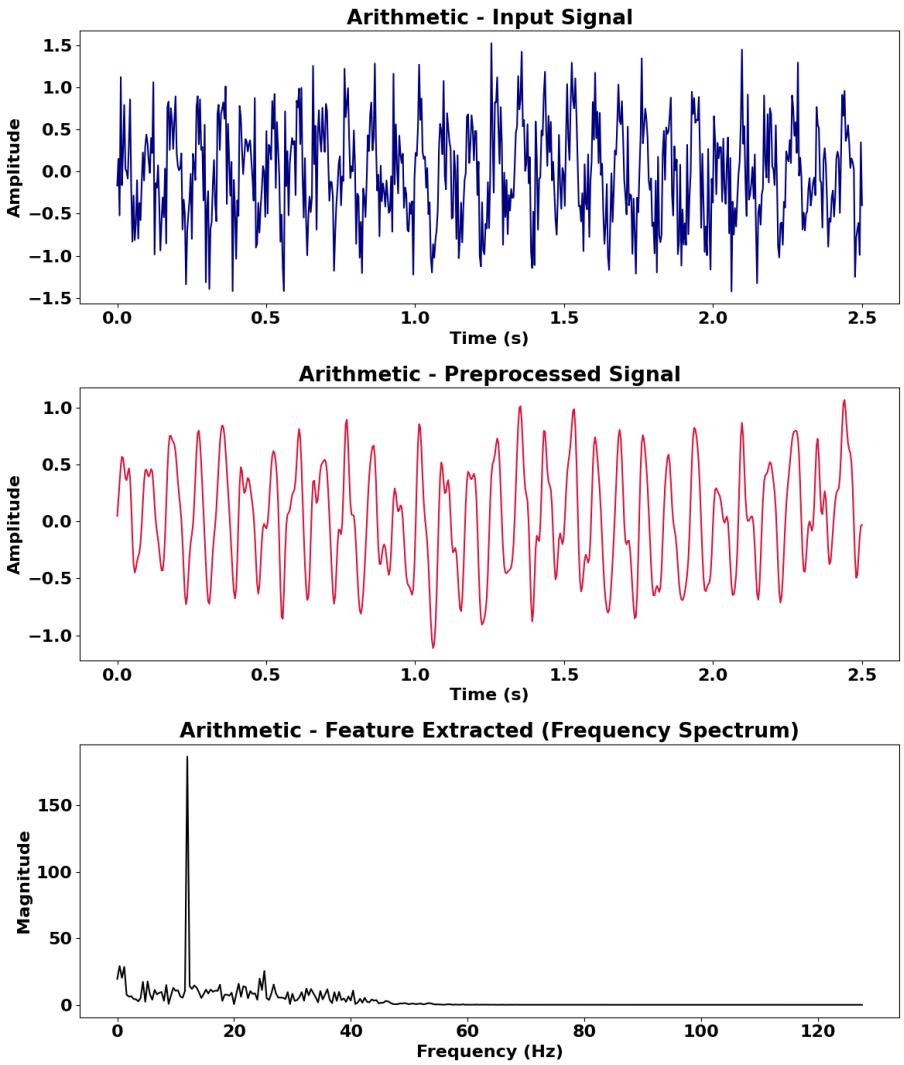


Figure 4: Output result of the suggested method on Dataset 1 for the Arithmetic Task Class

Figure 5shows the output result of the suggested method on Dataset 1 for the Mirror Class.

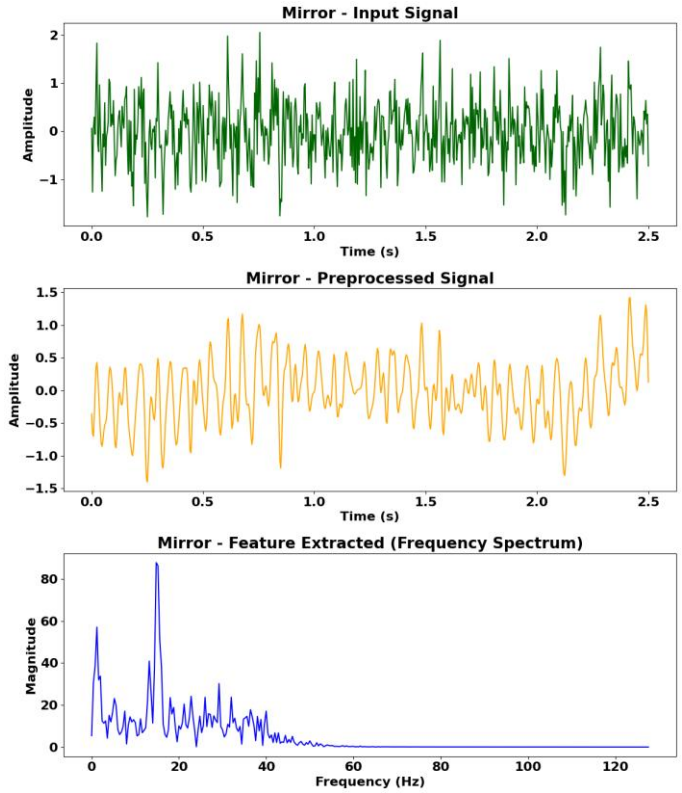


Figure 5: Output result of the suggested method on Dataset 1 for the Mirror Class

Figure 6 shows the output result of the suggested method on Dataset 1 for the Stroop Class.

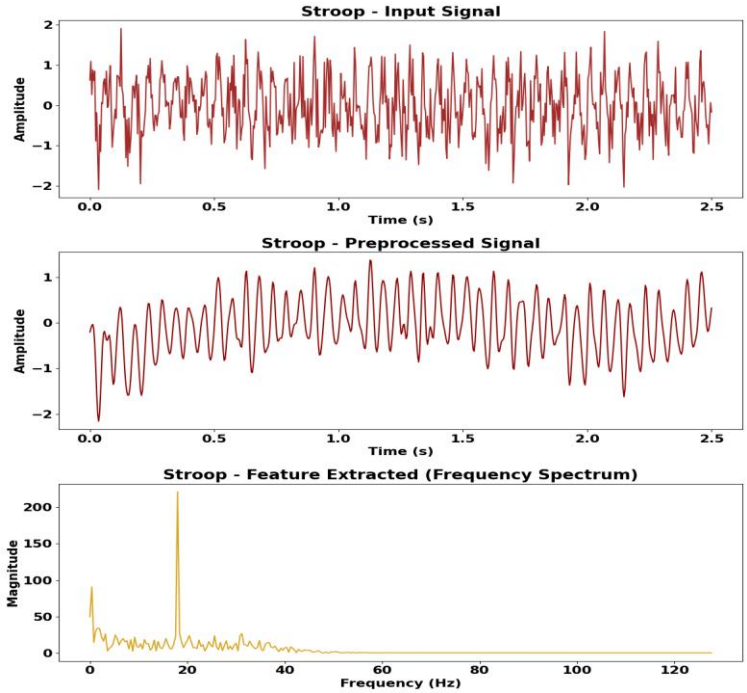


Figure 6: Output result of the suggested method on Dataset 1 for the Stroop Class

Figure 7 shows the output result of the suggested method on Dataset 1 for the Relax Class.

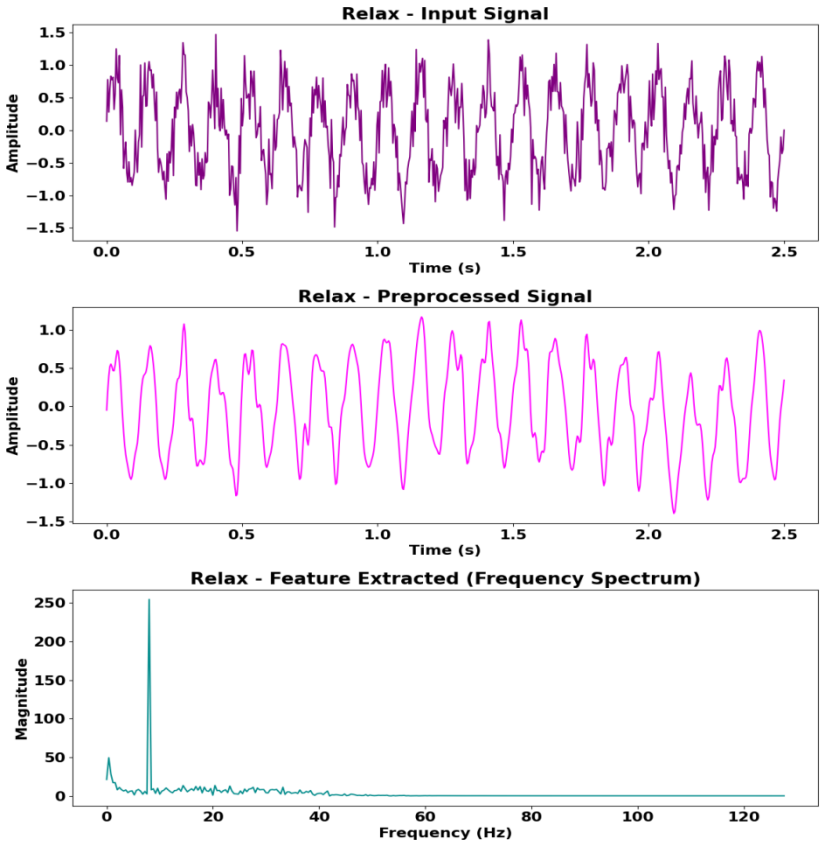


Figure 7: Output result of the suggested method on Dataset 1 for the Relax Class

Figure 8 shows the (a) Confusion matrix, (b) Correlation matrix, and (c) Dataset distribution.

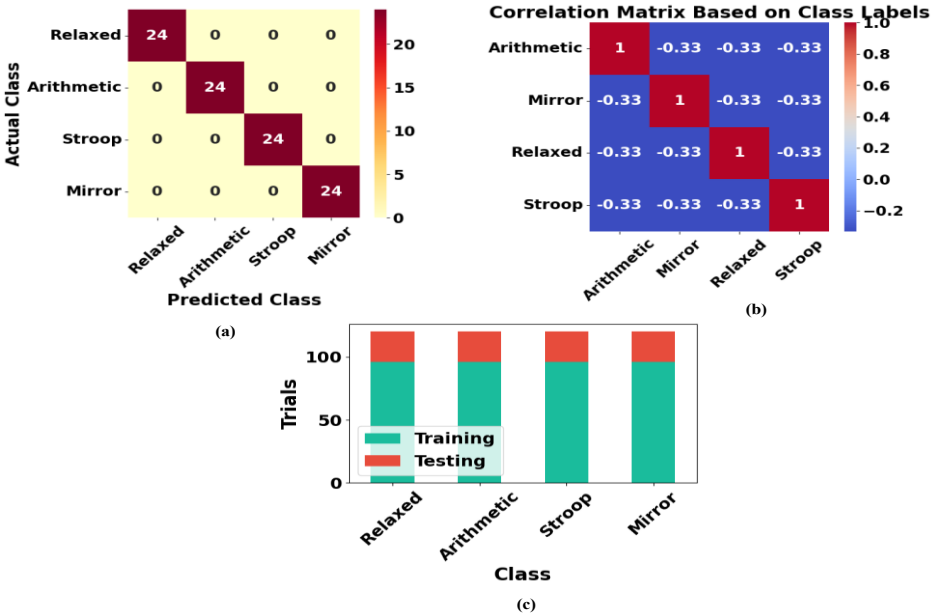


Figure 8: (a) Confusion matrix; (b) Correlation matrix; (c) Dataset distribution

Figure 8 presents a summary of classification performance across four task classes: cognitive tasks (relaxed), arithmetic, Stroop, and mirror. Figure 8 (a) The confusion matrix indicates the highest accuracy in classification as all 24 samples per class are accurately predicted, and none were misclassified, which implies that the model is performing well and it is easily separable into various classes. The correlation matrix (based on class labels) in Figure 8(b) shows strong self-correlation (1.0) along the diagonal and moderate negative correlations (−0.33) between classes, indicating balanced and mutually exclusive distributions. In Figure 8(c), the bar chart shows that they are provided with an equal number of trials in each class, with most time spent in training and a smaller fraction in testing. In general, the findings indicate a balanced distribution of data, high discriminative ability,

and strong classification scores across all four task conditions. Figure 9 shows the (a) Group distribution, (b) Sample counts, as well as (c) Frequency histogram.

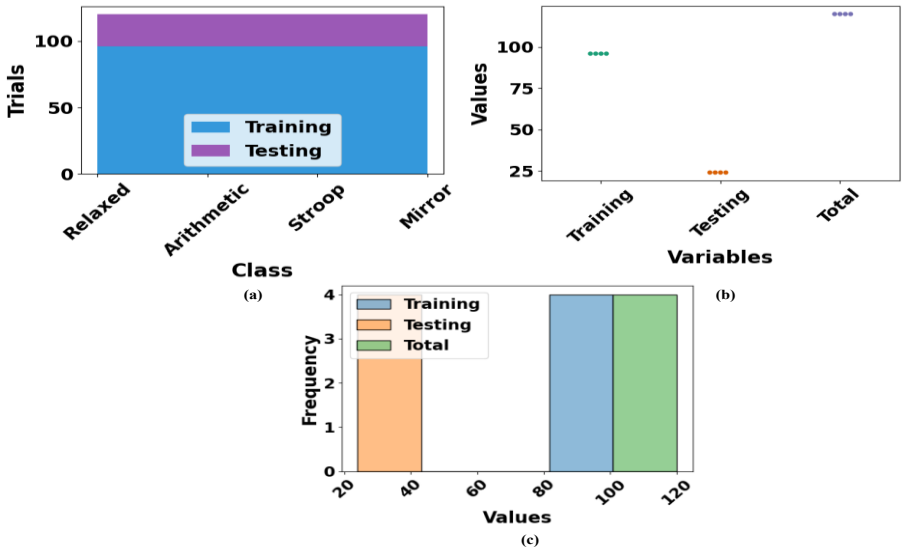


Figure 9: (a) Class distribution; (b) Sample counts; (c) Frequency histogram

Figure 9 shows how the trials are distributed in the various classes and dataset partitions. Figure 9(a) The stacked bar chart shows the number of training and testing trials of each class: Relaxed, Arithmetic, Stroop, and Mirror. The larger part is taken up by training, and the smaller part is played by testing, which implies that a train-test split with equal class representation can be expected. Figure 9(b): The scatter plot is a comparison of aggregate counts in Training, Testing, and Total samples. It is rather clear that training samples are significantly larger than test samples, and their combination is the outcome of these two. The histogram in Figure 9(c) is a summary frequency distribution of the values in the categories Training, Testing, and Total counts, with totals that are similar across the categories. On the whole, the visualization demonstrates equal classes and the appropriate division of the datasets, which enables reliable judgments and generalizations about the models. Figure 10 is an illustration of a (a) Scatter; (b) Heat map; (c) ECDF plot.

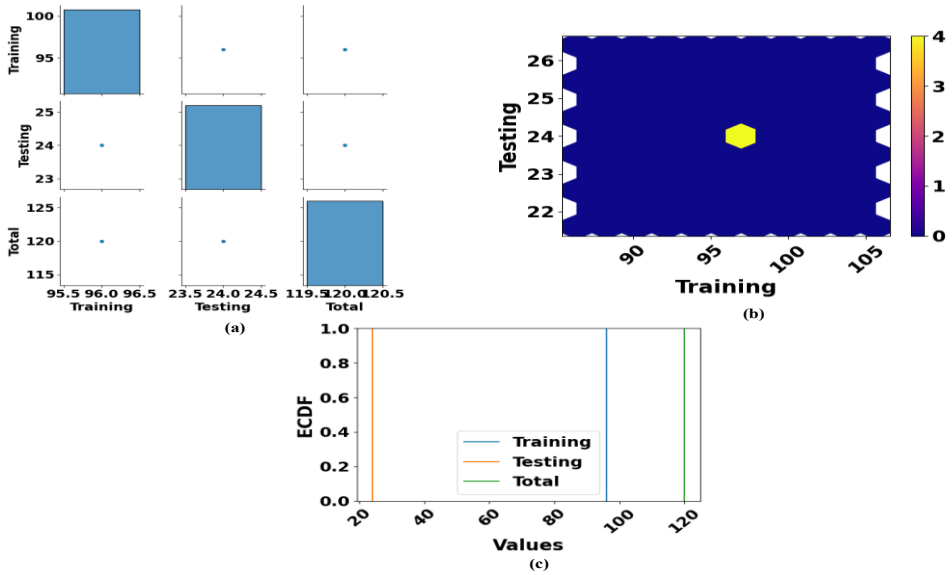


Figure 10: (a) Scatter matrix; (b) Heatmap; (c) ECDF plot

Figure 10 represents a statistical visualization of the dataset partitions. Figure 10(a) The scatter matrix shows the two-way correlation of training, testing, and the total number of samples. Diagonal plots present the distributions of the values, and off-diagonal plots show the uniform linear associations, meaning that Total equals the sum of Training along with Testing. Figure 10(b) The heatmap visualizes the density of distribution of Training and Testing values. A single bright point will mark a concentration of the information points, which can be interpreted as an invariable, fixed, and balanced distribution of the size of partitions. Figure 10(c) the plot of the

empirical cumulative distribution function (ECDF) of Training, Testing, and Total counts. All the curves have a sharp step, indicating discrete, constant values rather than spread distributions. In general, the visualizations confirm the stable allocation of data, well-developed proportional consistency, and deterministic splitting appropriate for controlled experimental analysis. The (a) Loss curves, (b) Accuracy curves, and (c) ROC curve are presented in Figure 11.

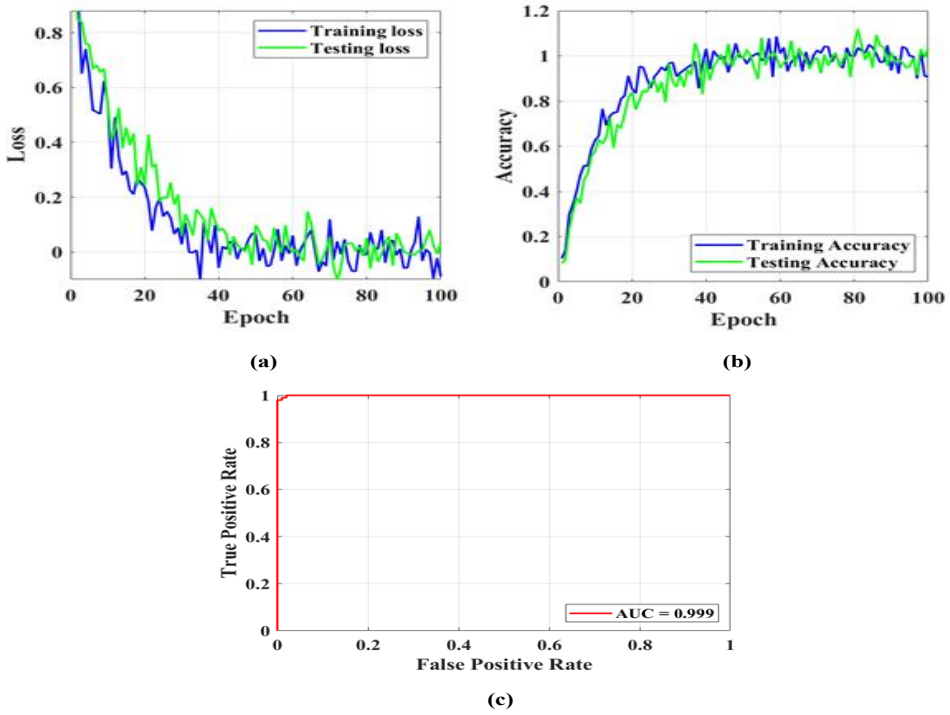


Figure 11: (a) Loss curves; (b) Accuracy curves; (c) ROC curve

Figure 11 shows model training performance and evaluation metrics over epochs. Figure 11(a) The loss curves indicate that both training and test loss reduce quickly in the first epochs, and then the trend flattens around zero. The fact that the curves are very close indicates minimal overfitting and good learning. Figure 11(b) shows the accuracy curves, i.e., the accuracy of both the training and test sets gradually approaches nearly 100 percent. The convergent trends are similar, indicating high generalization ability and convergent stability. The ROC curve in Figure 11(c) depicts the true positive rate versus the false positive rate. It is close to the upper-left corner, and its AUC of 0.999 is a good indication of the strong discriminative power. The findings indicate the high predictive accuracy, efficiency optimization, and high classification reliability during training and testing. Table 5 summarizes the performance of the proposed method on Dataset 1 compared to other approaches.

Table 5: Performance comparison of the suggested approach on Dataset 1

Metrics / Methods	VGGish-CNN [16]	KRAFS-ANet [17]	1D-CNN [18]	U-AGGDCNet+SAO [19]	ISMO-WPT-DCNN [20]	DD-SHTNNt+CEO(Proposed)
Accuracy(%)	90.4	92.1	94.3	93.6	91.7	99.3
Sensitivity(%)	85.6	90.6	88.6	89.5	91.5	99.1
Specificity(%)	90.6	89.3	86.4	87.4	91.8	99.1
Precision(%)	92.6	91.5	90.5	89.4	88.5	99.1
Recall(%)	90.6	91.5	89.6	88.4	83.7	99.1
F1- score(%)	84.7	89.6	88.4	91.6	90.4	99.1

Table 5 compares the results of different types of EEG data on SD with Dataset 1. The DD-SHTNNt+CEO model is the highest-ranked among all the measures, with an accuracy of 99.3 percent, which is significantly

higher than VGGish-CNN (90.4 percent), KRAFS-ANet (92.1 percent), 1D-CNN (94.3 percent), U-AGGDCNet+SAO (93.6 percent), and ISMO-WPT-DCNN (91.7 percent). The proposed method has a sensitivity, specificity, and precision of 99.1 percent, recall, and F1-score, compared with other models, such as sensitivity (85.6-91.5 percent) and specificity (86.4-91.8 percent). These findings show that the suggested method is more reliable and accurate in SD using EEG than the existing benchmark models.

4.3.2. Performance analysis of Dataset 2

The following section summarizes the performance evaluation results achieved for Dataset 2, and the figure 12 shows the visualization of (a) Calm and (b) Stress Emotional State Clusters Comparison on the Dataset 2.

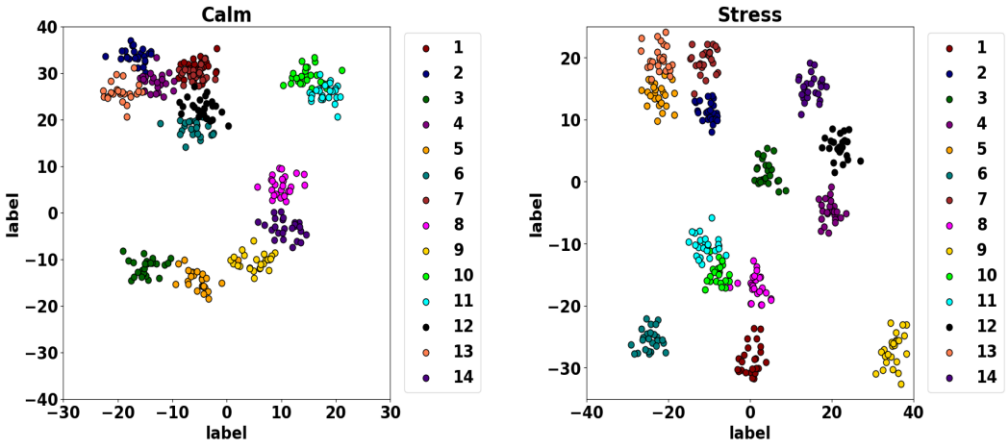


Figure 12: Visualization of (a) Calm and (b) Stress Emotional State Clusters Comparison on the Dataset 2

Figure 12 represents two-dimensional cluster distributions of the emotional states of the DEAP dataset. In Figure 12(a), Calm condition, the data points are easily defined and clustered into tight groups, indicating consistent and steady patterns of features among the subjects. The majority of groups are clear and show little overlap, suggesting less variability in physiological measures in calm states. According to Figure 12(b), the clusters of stress conditions are more dispersed and scattered in the feature space. Although the distance between them remains apparent, the distribution is more diffuse, reflecting greater dissimilarity in the responses to stress. In general, the visualization demonstrates evident structural contrast between calm and intense emotional pictures. Figure 13 shows the (a) correlation matrix, (b) confusion matrix, as well as (c) dataset distribution.

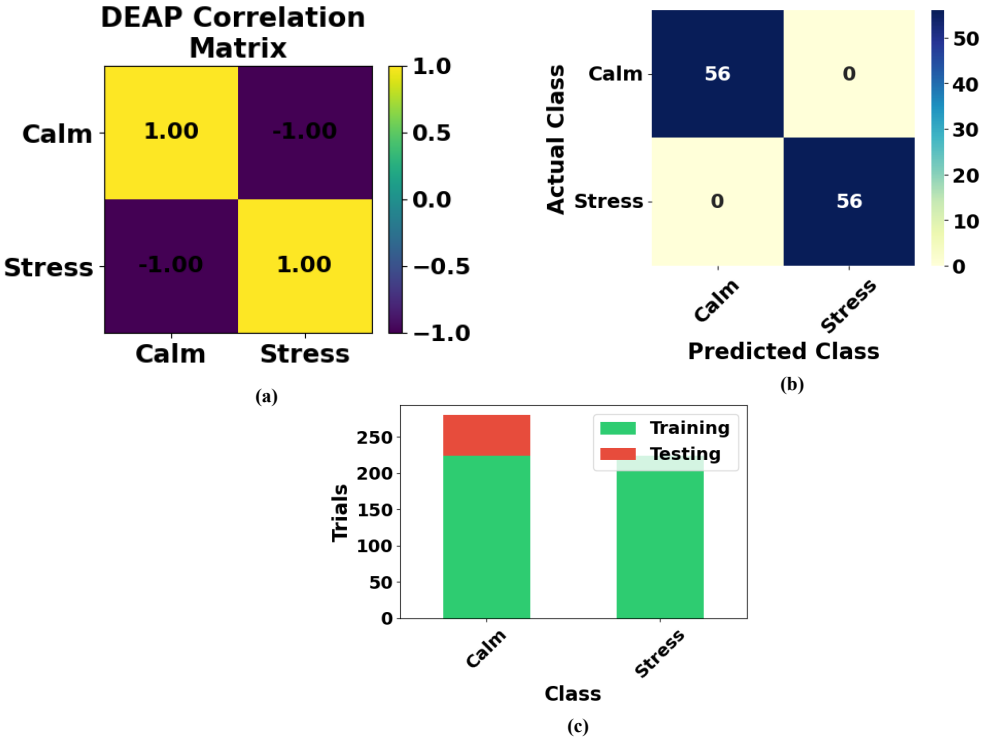


Figure 13: (a) Correlation matrix; (b) Confusion matrix; (c) Dataset distribution

Figure 13 provides a summary of the classification analysis of the DEAP Calm–Stress dataset. Figure 13 (a) The correlation matrix shows that the Calm and Stress classes have a negative correlation of (-1.00) with each other and a self-correlation of (1.00), which denotes that the labels are all divided, and the correlation exists in the opposite direction. Figure 13(b) illustrates a confusion matrix in which the sample is perfectly classified: Calm and Stress are correctly classified, and the remaining samples are not misclassified. This demonstrates 100% accuracy and high discriminative ability of the model. Figure 13(c) shows the distribution of the data in the bar chart: the same number of classes is used, with more in the training category and fewer in the testing category. Summing up, the visualizations attest to a clear segregation of classes, an equal distribution of data, and extremely dependable model output in the process of emotional state differentiation. Figure 14 shows the (a) Class distribution, (b) trial relation, and (c) statistical spread.

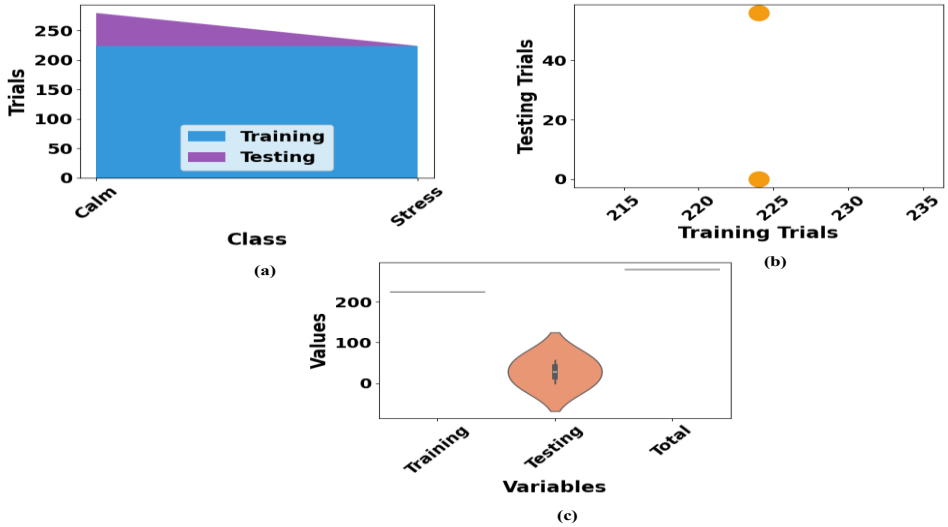


Figure 14: (a) Class distribution, (b) trial relation, (c) statistical spread

Figure 14 illustrates how the Calm and the Stress EEG experiments were distributed to develop the model. The sizes of the training and test samples for each class are shown in Figure 14(a). The Calm and Stress classes have approximately 270 and 50 training and testing trials, respectively, which leads to a slight imbalance between the classes. Figure 14(b) shows the relationship between training and testing trials, where the training samples are much larger than the testing samples in both categories. Figure 14(c) illustrates the statistical distribution of the trial values in a violin plot, where the total trial counts are higher in the training than in the testing, whereas the total number of trials represents both the training and testing. On the whole, the dataset has sufficient training samples and relatively small testing information. Figure 15 shows the (a) Dataset distribution table; (b) Class balance.

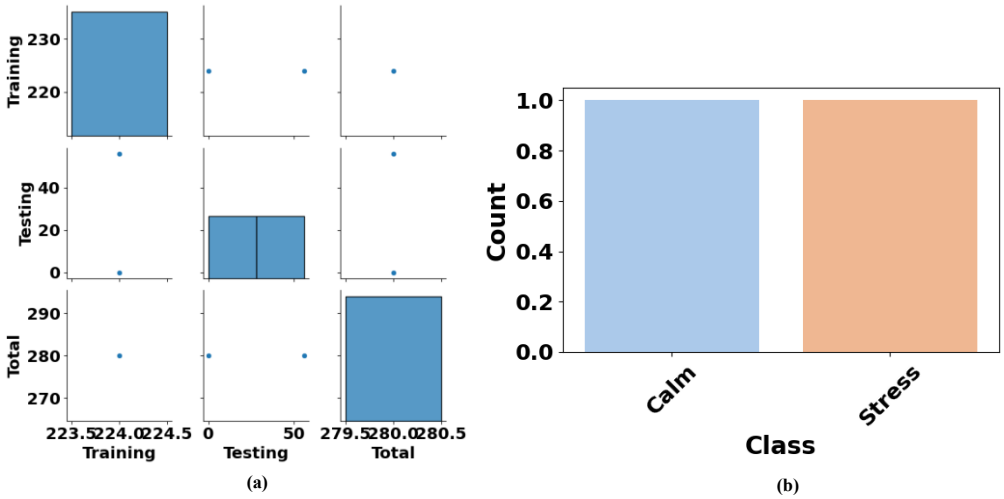


Figure 15: (a) Dataset distribution matrix; (b) Class balance

Figure 15(a) depicts the two-way distribution table of Training, Testing, and Total samples. Individual value ranges are represented with the use of diagonal plots, and split consistency is represented with the use of off-diagonal scatter plots. The points are also close together, indicating that the sample distributions are similar and that the difference between the purchased items is insignificant. It shows that the dataset is balanced, with equal

numbers of training and test samples. Figure 15 (b) The bar chart shows the distribution of classes of Calm and Stress categories. The heights of both bars are almost the same, indicating a balanced representation of the classes. This type of uniformity minimizes bias in model training and enhances the reliability of performance evaluation results. The (a) Histogram distribution, (b) ECDF curves, and (c) density map are depicted in Figure 16.

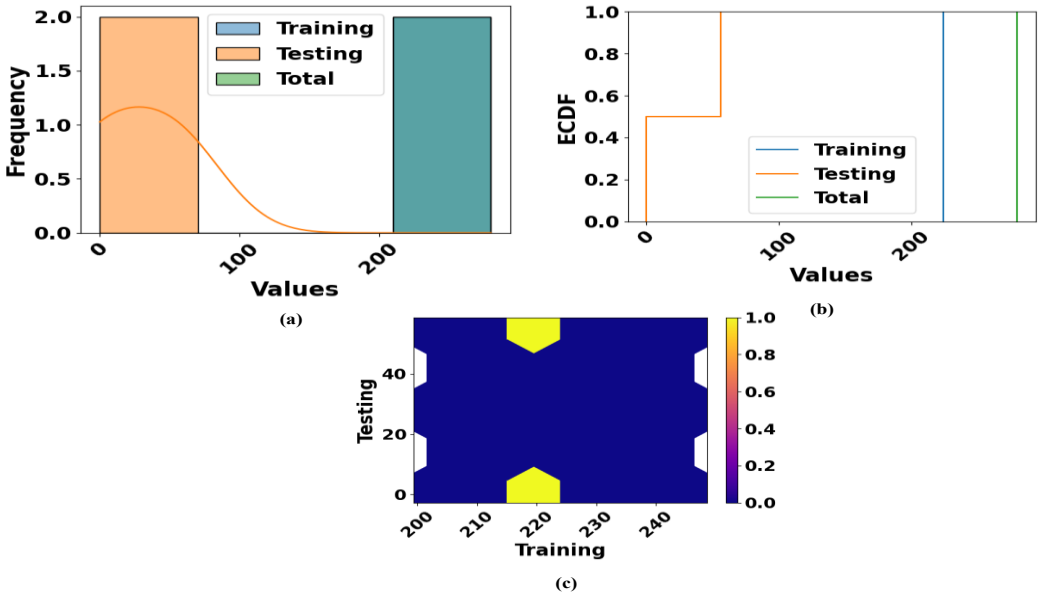


Figure 16: (a) Histogram distribution, (b) ECDF curves, (c) density map

Figure 16 shows the statistical distributions of the training, testing, and total trials. Figure 16 (a) presents a histogram with density estimation, and it can be seen that training values are more concentrated at the higher ranges compared to the values of the test. The entire distribution reflects the sum of the frequency spread, which implies that there is dominance of training samples. Figure 16(b) shows that the cumulative probability of testing increases rapidly due to the limited number of samples in the training set, while the full curves are slower at larger values. Figure 16(c) is a density-based contour/hexbin plot of training and test trials, illustrating clustering patterns and intensity levels. The brighter areas reflect the high concentration of trial combinations, which validate the imbalance and disparity in distribution between the sets used to develop and evaluate the model. Figure 17 illustrates the (a) Loss curves, (b) trends of accuracy,and (c) ROC curve.

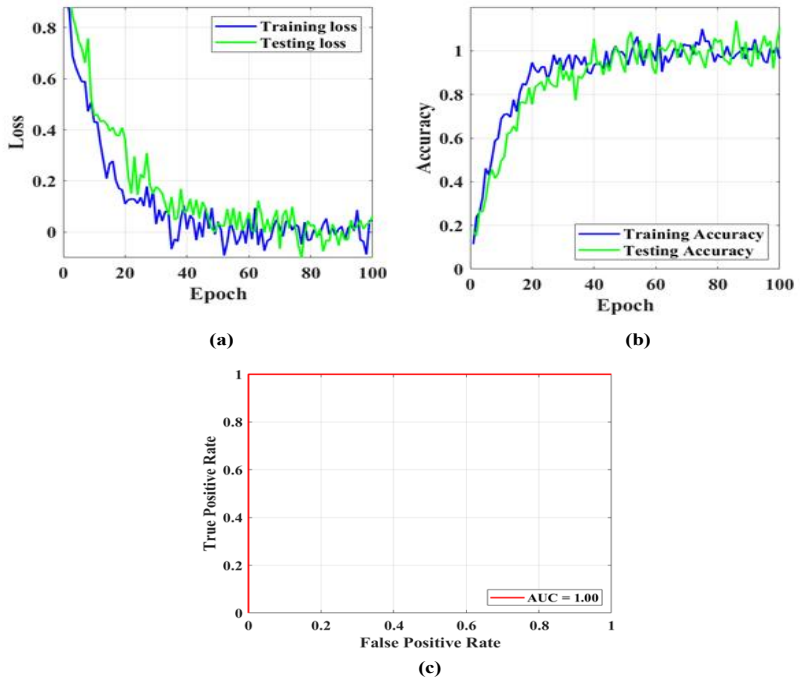


Figure 17: (a) Loss curves, (b) accuracy trends, (c) ROC curve

Figure 17 presents the measures of training performance and assessment of the proposed model. Figure 17(a) illustrates the training and testing loss curves at the 100 th epoch. Both losses decline sharply during the initial epochs to very low values, indicating they are good learners and not overfitting. The trends in training and test accuracy are plotted in Figure 17(b). It gradually becomes extremely accurate in the initial stages and reaches 100, which is a testament to strong generalization and consistent performance when applied to data that have never been encountered before. Figure 17(c) shows that the ROC curve has an AUC of 1.00 in the upper-left region of the curve. This implies perfect classification performance, with high true positives and low false positives. Overall, the model converges reliably, is accurate, and has high discriminative power. Table 6 presents the performance analysis of the proposed method on Dataset 2 and demonstrates that it can be successfully applied across various classification metrics.

Table 6: Performance comparison of the suggested technique with Dataset 2

Metrics / Methods	U-AGGDCNet+SAO [19]	ISMO-WPT-DCNN [20]	Stress Net [21]	ECNN-LSTM [22]	D-RNN-BiLSTM [23]	DD-SHTNNt+CEO(Proposed)
Accuracy(%)	90.5	89.3	88.4	92.1	91.5	99.3
Sensitivity(%)	92.4	91.4	90.4	89.4	88.5	99.1
Specificity(%)	92.5	89.3	84.2	88.4	90.4	99.1
Precision(%)	85.3	89.8	91.5	85.3	90.4	99.1
Recall(%)	86.4	91.7	90.5	89.4	89.7	99.1
F1- score(%)	84.6	86.8	85.4	90.4	91.6	99.1

Table 6 describes the performance of various models in Dataset 2 in SD. The other models have lower accuracies, including U-AGGDCNet+SAO, ISMO-WPT-DCNN, StressNet, ECNN-LSTM, and D-RNN-BiLSTM, with accuracies of 90.5, 89.3, 88.4, and 91.5, respectively. In the same manner, the suggested model is highly sensitive, specific, precise, and recalls, with an F1-score of 99.1. In comparison, the current techniques have a low sensitivity of 88.5%-92.4, a specificity of 84.2%-92.5, a precision of 85.3%-91.5, a recall of 86.4%-91.7, and an F1-score of 84.6%-91.6, indicating the validity of the suggested framework.

4.3.3. Comparison of the performance of the suggested method between the two databases

This section provides a detailed examination of the proposed strategy across both datasets. Table 7 illustrates the computational time as well as error rate achieved by the proposed approach and presents a detailed comparison with several existing techniques to demonstrate its efficiency and effectiveness.

Table 7: Comparison of Methods Based on Computational Time along with Error Rate

Methods	Computational time (sec)	Error rate (%)
VGGish-CNN [16]	0.80	7.9
KRAFS-ANet [17]	0.83	7.4
1D-CNN [18]	0.78	8.0
U-AGGDCNet+SAO [19]	0.79	8.5
ISMO-WPT-DCNN [20]	0.81	8.7
StressNet [21]	0.84	8.4
ECNN-LSTM [22]	0.86	7.7

D-RNN-BiLSTM [23]	0.75	7.8
DD-SHTNNt+CEO(Proposed)	**0.22**	**0.3**

Table 7 compares the methods with respect to computation time and stress-detection error rates using EEG. VGGish-CNN requires 0.80 s and an error rate of 7.9, and 1D-CNN requires 0.78 s and 8.0 error rate. U-AGGDCNet + SAO will require 0.79 s and an error rate of 8.5%. Similarly, ISMO-WPT-DCNN and StressNet have 0.81s (8.7) and 0.84 s (8.4 deaths), respectively. ECNN-LSTM and D-RNN-BiLSTM required 0.86 s (7.7%) and 0.75 s (7.8%), respectively. It also has a much more efficient and precise suggested DD-SHTNNt+CEO, which has 0.3% error and requires much less computer time (0.22 s) than it does. The results of the 5-fold cross-validation (CV) are presented in Table 8 and confirm that the suggested approach yields consistent results across all data splits.

Table 8: 5-Fold CV Accuracy Results of both datasets

Fold	Accuracy (%)	Accuracy (%)
	Dataset 1	**Dataset 2**
Fold 1	99.3	99.4
Fold 2	99.3	99.2
Fold 3	99.3	99.3
Fold 4	99.2	99.3
Fold 5	99.4	99.4
Average	99.3	99.3
Mean ± SD	99.3 ± 0.07	99.3 ± 0.07

Table 8 shows the performance of the proposed model on the two datasets using 5-fold CV, indicating high accuracy and reliability. In Dataset 1, the five-fold scores are 99.3, 99.3, 99.3, 99.2, and 99.4, respectively. On the same note, Dataset 2 has accuracies of 99.4%, 99.2%, 99.3%, 99.3%, and 99.4% across Fold 1-5. The first one is the mean accuracy across the two datasets, which is 99.3, indicating that the model behaves consistently and that the results are not different across splits. Moreover, the standard deviation and mean values of 99.34 ± 0.07 indicate high stability and an insignificant change in the model during cross-validation, suggesting strong generalization to EEG-based stress detection tasks.The optimization algorithms are compared in terms of performance as presented in Table 9.

Table 9: Performance comparison of optimization algorithms

Optimizer	Convergence Rate	Iterations to Converge	Computational Time (s)	Memory Usage (MB)	Accuracy (%)
TWO [31]	0.024	139	162.77	912	99.01
MSSO-AO [32]	0.030	123	211.63	1251	99.21
DBPSO [33]	0.017	221	187.42	906	98.34
IFO [34]	0.033	90	192.30	1083	99.22
CEO(Proposed)	0.046	71	151.20	828	99.78

Table 9 provides a comparison of various optimization algorithms based on their convergence rate, convergence iterations, computational time, memory consumption, and accuracy. MSSO-AO improves convergence to 0.030 with 123 iterations, but requires a higher 211.63 s time and 1251 MB memory, reaching 99.21% accuracy. DBPSO shows a lower convergence rate of 0.017, needs 221 iterations, 187.42 s, 906 MB, and achieves 98.34% accuracy. IFO records 0.033 convergence, 90 iterations, 192.30 s, 1083 MB, and 99.22% accuracy. The proposed CEO performs best with the highest convergence rate,0.046, minimum 71 iterations, lowest 151.20 s, 828 MB, and the highest 99.78% accuracy.

4.4. Statistical test

The early EEG-based stress detection and analysis framework has been developed and comprehensively evaluated using the Kruskal–Wallis (H), Friedman (FT), and Wilcoxon Signed-Rank (WSR) tests to determine the statistical significance of performance differences among various classification methods. The normalcy and appropriateness of the acquired performance indicators were further assessed using the Shapiro-Wilk (SW) and Kolmogorov-Smirnov (KS) tests. Table 10 presents the statistical results comparing the variances of the proposed EEG-based SD model with those of existing methods. The findings show that the suggested model is more reliable, stable, and effective for the practical interpretation of EEG signals and early SD.

Table 10: Statistical research comparison of the suggested strategy and the current methods

Methods	SW Test p-Value	WSR test / U-test p-Value	H-test p-Value	KS test p-value	FT p-Value	Mean	Standard Deviation	Variance Inflation Factor (VIF)
VGGish-CNN [16]	0.442	0.339	0.85	0.090	0.091	278,753.13	3,376.39	1.85
KRAFS-ANet [17]	0.348	0.257	0.82	0.089	0.090	460,543.45	2,257.67	1.89
1D-CNN [18]	0.330	0.189	0.88	0.082	0.084	86,267.57	3,174.76	1.84
U-AGGDCNet+SAO [19]	0.420	0.267	0.84	0.086	0.083	384,845.78	2,358.80	1.90
ISMO-WPT-DCNN [20]	0.356	0.351	0.83	0.083	0.087	282,291.80	1,173.78	1.91
StressNet [21]	0.358	0.467	0.90	0.084	0.088	69,538.49	5,338.41	1.92
ECNN-LSTM [22]	0.239	0.340	0.92	0.091	0.078	65,447.89	1,345.30	1.87
D-RNN-BiLSTM [23]	0.321	0.281	0.86	0.089	0.081	68,345.57	5,389.18	1.82
DD-SHTNNt+CEO (Proposed)	<0.001	<0.001	<0.001	<0.001	<0.001	65,867.27	6,763.58	1.001

Table 10 presents a statistical comparison of the suggested DD-SHTNNt+CEO system and the current methods. The statistical results of the suggested model are very important, SW test p-value less than 0.001, WSR/U-test p-value less than 0.001, H-test p-value less than 0.001, KS test p-value less than 0.001, and FT p-value less than 0.001, which are very reliable. It indicates a standard deviation of 6,763.58, a mean of 65,867.27, and a VIF of 1.001, which suggests a low level of multicollinearity. There are others, including VGGish-CNN (mean 278,753.13, VIF 1.85) and KRAFS-ANet (mean 460,543.45, VIF 1.89), which are higher since they are statistically significant. Overall, the suggested methodology is more stable and more powerful statistically.

4.5. Ablation study

An ablation study evaluated the contribution of each module of the proposed DD-SHTNNt+CEO-based architecture to early Stress recognition and assessment using EEG signals. The results presented in Table 11 show that each component is essential for increasing the overall performance of the system. Each module enhances the model's accuracy and stability. Also, the analysis shows that the combined structure carries increased generalization capabilities and is more stable. Among other results, this means that the developed solution provides a valid and efficient method for detecting and analyzing early stress using EEG signals.

Table 11: Ablation study results

Model Configuration	S-PDM-3DMD	Q-CFT	DHNN	D-STT	CEO	Accuracy (%)	Precision (%)	Recall (%)	F1-Score (%)
Baseline (Without CEO)	✘	✘	✔	✘	✘	84.4	82.3	81.9	82.1
Without S-PDM-3DMD	✘	✔	✔	✔	✘	89.8	86.4	88.2	88.9
Without Q-CFT	✔	✘	✔	✔	✘	91.3	90.2	87.5	85.8
DHNN Only	✔	✔	✔	✘	✘	88.9	84.8	85.5	82.2
D-STT Only	✔	✔	✘	✔	✘	88.1	87.1	84.9	86.9
DHNN + D-STT (No CEO)	✔	✔	✔	✔	✘	92.6	90.5	90.4	91.2
DHNN + **CEO**	✔	✔	✔	✘	✔	94.6	91.8	90.6	89.9
D-STT + **CEO**	✔	✔	✘	✔	✔	91.0	88.4	87.3	86.2

Full Model (DD-SHTNNt+CEO)	✔	✔	✔	✔	✔	**99.3**	**99.1**	**99.1**	**99.1**

Table 11 presents an ablation study evaluating how different components affect model performance. The lowest results are for the baseline (without the CEO): 84.4% accuracy, 82.3% precision, 81.9% recall, and 82.1% F1-score. Removing S-PDM-3DMD improves results to 89.8% accuracy, 86.4% precision, 88.2% recall, and 88.9% F1. Without Q-CFT, performance becomes 91.3% accuracy, 90.2% precision, 87.5% recall, 85.8% F1. DHNN only gives 88.9% accuracy, while D-STT only yields 88.1% accuracy. A combination of DHNN + D-STT increases to 92.6% accuracy, 90.5% precision, 90.4% recall, 91.2% F1. The addition of the CEO increases the accuracy to 94.6 percent. The full model (DD-SHTNN+CEO) achieves the best performance: 99.3% accuracy, 99.1% precision, 99.1% recall, and 99.1% F1-score.

4.6. Discussion

The effectiveness of the suggested framework, based on DD-SHTNNt+CEO, is demonstrated by the results of experiments on detecting early stress from EEG signals. To achieve complete model validation across various experimental results, the model was developed in as well as tested on two benchmark datasets, SAM 40 and DEAP. The performance analysis demonstrates that the proposed strategy outperforms other deep learning and hybrid models across a range of evaluation measures. In Dataset 1, the model's accuracy reached 99.3, and the values of sensitivity, specificity, precision, recall, and F1-score were 99.1 each. Likewise, the model retained its high accuracy of 99.3% across Dataset 2 and remained the best across all statistical metrics compared to the benchmark methods VGGish-CNN, KRAFS-ANet, StressNet, ECNN-LSTM, and D-RNN-BiLSTM. The confusion matrices of the two datasets revealed that the model discriminated without error, indicating that it effectively distinguishes between stress and non-stress EEG patterns. The ROC curves also indicated that the model is highly discriminative, with an AUC value of almost 1. The computational efficiency of the suggested model is also mentioned, as is its performance in classification. It had very low computational time, an error rate of 0.3, and a framework that was also very low, meaning it can be utilized in real-time stress-monitoring systems. The 5-fold cross-validation findings were also supportive of the model's strength, with a mean of 99.3 and a standard deviation of 0.07, both very low, indicating that the model is powerful across different data splits. Further, statistical significance tests, including SW, WSR, Kruskal-Wallis, Kolmogorov-Smirnov, and FT, indicate that the proposed solution is statistically superior to the current procedures. The ablation study also emphasized the effectiveness of incorporating all elements of the framework, as the complete DD-SHTNNt+CEO model achieved the best performance compared to partial models. On the whole, the findings show that the suggested framework provides a low-risk, effective, and most precise approach to the early identification of stress using EEG.

Acknowledgement

This paper was supported by Sunchon National University Glocal University Project Fund in 2025. (Grant number: 2025-0020)

5. Conclusion

In this manuscript, the suggested DD-SHTNNt+CEO framework is successfully implemented for effective early SD and evaluation using EEG signals. The EEG signals obtained from the SAM40 and DEAP datasets are first preprocessed using the S-PDM-3DMD method to eliminate noise and enhance signal quality. The Q-CFT technique is then applied to extract discriminative features to describe the significant patterns of stress. These characteristics are subsequently provided to the DD-SHTNNt model, which combines a DHNN with a D-STT to achieve accurate stress classification. Moreover, the CEO algorithm optimally adjusts the network's parameters, thereby enhancing classification precision, convergence rate, stability, and the generalization ability of the proposed structure. The suggested framework is fully implemented in Python, enabling efficient model development and evaluation. Experimental results demonstrate that the suggestedDD-SHTNNt+CEO framework achieves a high detection accuracy of 99.3%, a specificity of 99.1%, and a recall of 99.1%, with a minimal error rate of 0.3%. These findings indicate that the suggested model is effective at separating stressful states from EEG signals. Further, the framework offers greater robustness, rapid convergence, and strong generalization, making it both a reliable and effective method for early SD.Future work may focus on validating the DD-SHTNNt+CEO framework on larger as well as more diverse EEG datasets, integrating multimodal physiological signals, enabling real-time stress monitoring, improving model interpretability, and developing lightweight architectures for wearable healthcare devices and practical clinical deployment.

References

1. Kamakshi, Kamini, and ArthiRengaraj. "Early detection of stress and anxiety based seizures in position data augmented EEG signal using hybrid deep learning algorithms." *IEEE Access* 12 (2024): 35351-35365.
2. Seo, Wonju, et al. "Deep learning approach for detecting work-related stress using multimodal signals." *IEEE Sensors Journal* 22.12 (2022): 11892-11902.

3. Li, Mi, et al. "Stress severity detection in college students using emotional pulse signals and deep learning." *IEEE Transactions on Affective Computing* (2025).
4. Kim, Hyoung-Gook, Dong-Ki Jeong, and Jin-Young Kim. "Emotional stress recognition using electroencephalogram signals based on a three-dimensional convolutional gated self-attention deep neural network." *Applied Sciences* 12.21 (2022): 11162.
5. Anik, Israq Ahmed, et al. "A robust deep-learning model to detect major depressive disorder utilizing EEG signals." *IEEE Transactions on Artificial Intelligence* 5.10 (2024): 4938-4947.
6. Gupta, Varun, et al. "A design of bat-based optimized deep learning model for EEG signal analysis." *Multimedia Tools and Applications* 82.29 (2023): 45367-45387.
7. Kakade, Mandar Nitin. "RosMS-ECDBTM: Efficient Channel Attention Enabled Distributed Deep Learning Model for Mental State Detection Using EEG Signal." *Neurocomputing* (2025): 131559.
8. Malviya, Lokesh, and Sandip Mal. "CIS feature selection based dynamic ensemble selection model for human stress detection from EEG signals." *Cluster Computing* 26.4 (2023): 2367-2381.
9. Jadhav, Akshay, et al. "Human stress detection from swcteeg data using optimised stacked deep learning model." *Doctoral Symposium on Human Centered Computing*. Singapore: Springer Nature Singapore, 2023.
10. Abidi, Mustufa Haider, et al. "EEGDepressionNet: A novel self attention-based gated DenseNet with hybrid heuristic adopted mental depression detection model using EEG signals." *IEEE Journal of Biomedical and Health Informatics* 28.9 (2024): 5168-5179.
11. Sletta, Øystein, et al. "Newly identified Phonocardiography frequency bands for psychological stress detection with Deep Wavelet Scattering Network." *Computers in Biology and Medicine* 178 (2024): 108722.
12. Barshutina, M., et al. "SERS substrates based on rose petal replicas for the oxidative stress detection." *Applied Surface Science* 626 (2023): 157281.
13. Kumar, Geethu S., and B. Ankayarkanni. "Leveraging Conv-XGBoost algorithm for perceived mental stress detection using Photoplethysmography." *Intelligence-Based Medicine* 11 (2025): 100209.
14. Hafeez, Muhammad Adeel, and Sadia Shakil. "EEG-based stress identification and classification using deep learning." *Multimedia Tools and Applications* 83.14 (2024): 42703-42719.
15. Malviya, Lokesh, and Sandip Mal. "A novel technique for stress detection from EEG signal using hybrid deep learning model." *Neural Computing and Applications* 34.22 (2022): 19819-19830.
16. Afify, Heba M., Kamel K. Mohammed, and Aboul Ella Hassanien. "Stress detection based EEG under varying cognitive tasks using convolution neural network." *Neural Computing and Applications* 37.7 (2025): 5381-5395.
17. Shikha, Shikha, DivyashikhaSethia, and S. Indu. "KRAFS-ANet: A novel framework for EEG-based stress classification using channel selection and optimized ensemble stacking." *International Journal of Machine Learning and Cybernetics* 16.5 (2025): 3359-3380.
18. Naren, J., and Mathiarasi Balakrishnan. "Stress detection using the phase controlled Bi-channel adaptive features from the brain EEG signals." *Computers in Biology and Medicine* 201 (2026): 111400.
19. Bamanikar, Ashvini, et al. "Early Stress Detection and Analysis Using EEG Signals-Based Uncertainty-Aware Gated Graph Decision Capsule Network with Snow Ablation Optimization." *Biomedical Materials & Devices* (2025): 1-25.
20. Dhake, Dipali, and Yogesh Angal. "Novel 2-D Wavelet-Based Spectral-Temporal Representation for Deep Learning Based Stress Detection Using EEG Signal." *Circuits, Systems, and Signal Processing* (2025): 1-23.
21. Mane, Swaymprabha Alias Megha, and Arundhati Shinde. "StressNet: Hybrid model of LSTM and CNN for stress detection from electroencephalogram signal (EEG)." *Results in Control and Optimization* 11 (2023): 100231.
22. Hamatta, Hatem SA, et al. "Genetic algorithm-based human mental stress detection and alerting in Internet of Things." *Computational Intelligence and Neuroscience* 2022.1 (2022): 4086213.
23. Joshi, Vaishali M., et al. "Deep BiLSTM neural network model for emotion detection using cross-dataset approach." *Biomedical Signal Processing and Control* 73 (2022): 103407.
24. Lee, Seongmin, SuwoongHeo, and Sanghoon Lee. "DMESH: A structure-preserving diffusion model for 3-D mesh denoising." *IEEE Transactions on Neural Networks and Learning Systems* 36.3 (2024): 4385-4399.
25. Hitzer, Eckhard. "Quaternion Fourier Transform." *Quaternionic Integral Transforms: A Machine-Generated Literature Overview*. Cham: Springer International Publishing, 2023. 1-58.
26. Guo, Yueling, et al. "Dual optimization approach in discrete Hopfield neural network." *Applied Soft Computing* 164 (2024): 111929.
27. Yu, En, et al. "Enhancing outdoor vision: Binocular desnowing with dual-stream temporal transformer." *Pattern Recognition* 170 (2026): 112075.
28. Wang, Rui, Zhengxuan Jiang, and Guowen Ding. "Cosmic Evolution Optimization: A Novel Metaheuristic Algorithm for Numerical Optimization and Engineering Design." *Mathematics* 13.15 (2025): 2499.
29. Ghosh, Rajdeep, et al. "SAM 40: Dataset of 40 subject EEG recordings to monitor the induced-stress while performing Stroop color-word test, arithmetic task, and mirror image recognition task." *Data in Brief* 40 (2022): 107772.

30. Koelstra, Sander, et al. "Deap: A database for emotion analysis; using physiological signals." *IEEE transactions on affective computing* 3.1 (2011): 18-31.
31. Gupta, Sonam, et al. "TOXGB: Teamwork Optimization Based XGBoost model for early identification of post-traumatic stress disorder." *Cognitive Neurodynamics* 16.4 (2022): 833-846.
32. Singh, Arjun, et al. "Archimedes optimization-based Elman Recurrent Neural Network for detection of post-traumatic stress disorder." *Biomedical Signal Processing and Control* 90 (2024): 105806.
33. Pankajavalli, P. B., and G. S. Karthick. "Improved Stress Prediction Using Differential Boosting Particle Swarm Optimization-Based Support Vector Machine Classifier." *Intelligent Sustainable Systems: Proceedings of ICISS 2021*. Singapore: Springer Singapore, 2021. 233-244.
34. Bhanja, N., et al. "Optimization of convolutional neural network for accurate stress detection using multimodal physiological signals." *South Eastern European Journal of Public Health* (2025): 5241-5255.